Available online at www.sciencedirect.com
SCIENCE DIRECT
Geochimica et Cosmochimica Acta 70 (2006) 2354–2370
Geochimica
www.elsevier.com/locate/gca

# Paleozoic ages and excess $^{40}Ar$ in garnets from the Bixiling eclogite in Dabieshan, China: New insights from $^{40}Ar/^{39}Ar$ dating by stepwise crushing

Hua-Ning Qiu [a,b,*], J.R. Wijbrans [b]

[a] *Key Laboratory of Isotope Geochronology and Geochemistry, Guangzhou Institute of Geochemistry, Chinese Academy of Sciences, P.O. Box 1131, 510640 Guangzhou, China*

[b] *Department of Isotope Geochemistry, Vrije Universiteit Amsterdam, De Boelelaan 1085, 1081 HV Amsterdam, The Netherlands*

Received 17 February 2005; accepted in revised form 14 November 2005

**Abstract**

The $^{40}Ar/^{39}Ar$ stepwise crushing technique is applied for the first time to date garnet from ultra-high-pressure metamorphic (UHPM) eclogites. Three garnet samples from the Bixiling eclogites analyzed by $^{40}Ar/^{39}Ar$ stepwise crushing yield regular, predictable age spectra, and a clear separation between excess $^{40}Ar$ and concordant plateau and isochron ages. All three age spectra begin with high apparent ages followed by step by step decreasing ages, and finally age plateaux with apparent ages in the range from $427 \pm 20$ to $444 \pm 10$ Ma. The data points constituting the age plateaux yield excellent isochrons with radiogenic intercept ages ranging from $448 \pm 34$ to $459 \pm 58$ Ma, corresponding to initial $^{40}Ar/^{36}Ar$ ratios from $292.1 \pm 4.5$ to $294.5 \pm 6.7$, statistically indistinguishable from the modern air. The high initial ages are interpreted to derive from secondary fluid inclusions containing excess $^{40}Ar$, whereas the plateau ages are attributed to gas from small primary fluid inclusions without significant excess $^{40}Ar$. The plateau ages are interpreted to approximate the time of garnet growth during initial UHPM metamorphism. Phengite analyzed by laser stepwise heating yielded a complicated two-saddle age spectrum with a scattered isochron corresponding to age of $463 \pm 116$ Ma and initial $^{40}Ar/^{36}Ar$ ratio of $1843 \pm 1740$ indicative of the presence of extraneous $^{40}Ar$ within phengite. These concordant isochron ages measured on minerals diagnostic of eclogite grade metamorphism strongly suggest that Dabie UHPM eclogites were first formed in the early Paleozoic, during the same event that caused the Qinling–Northern Qaidam Basin–Altyn Tagh eclogites.


## 1. Introduction

The Dabieshan and Sulu terranes in central-eastern China form the largest occurrence of ultra-high-pressure metamorphic (UHPM) rocks in the world (Fig. 1) (Xu et al., 1992; Zhang et al., 1995; Ye et al., 2000, 2001, 2002; Xu et al., 2003) and, as a consequence, have become the focus of intense geological research on the characteristics of UHP metamorphism (Li et al., 1993; Okay et al., 1993; Hacker and Wang, 1995; Liu et al., 1995; Cao and Zhu, 1996; Chavagnac and Jahn, 1996; Hacker et al., 1998; Yang and Jian, 1998; Cong and Wang, 1999; Yang et al., 2002).

The pressure–temperature–time (PT*t*) path of the UHPM rocks has been constrained by geobarometry and isotopic techniques. Metamorphic temperatures and pressures of ca. 600–1140 °C and 18–67 kbar were estimated (Okay, 1993; Zheng, 1993a,b; Zhang et al., 1995; Xiao et al., 2000). Extremely deep burial is demonstrated by ubiquitous coesite and local diamond (Xu et al., 1992, 2003; Ye et al., 2001). Subduction depths of greater than 200 km were inferred (Ye et al., 2000). Sm–Nd and Rb–Sr isochron dating of eclogites from both the Dabieshan and the Sulu terranes yielded consistent results of 240–220 Ma (Li et al., 1994; Chavagnac and Jahn, 1996).

* Corresponding author. Fax: +86 20 85290130.
*E-mail address:* qiuhn@gig.ac.cn (H.-N. Qiu).

0016-7037/$ - see front matter © 2006 Published by Elsevier Inc.
doi:10.1016/j.gca.2005.11.030

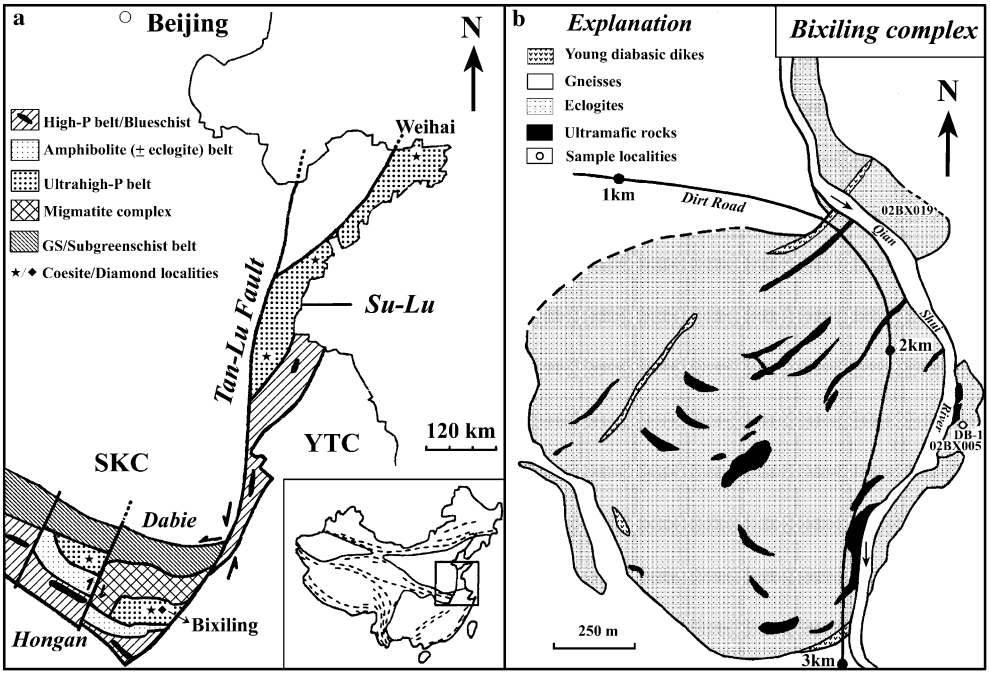


Fig. 1. Sketch maps of simplified geology: (a) Dabie–Sulu Terranes: SKC, Sino-Korean Craton; YTC, Yangtze Craton (please refer Fig. 10 for the latitude and longitude) (b) Bixiling. Modified after Zhang et al. (1995) (GPS locations of 02BX005 and 02BX019 are 50R0431671-UTM3400149 and 50R0431525-UTM3400695, respectively).

In contrast, $^{40}Ar/^{39}Ar$ dating of phengites yielded clearly older ages than the results obtained by other techniques. Giorgis et al. (2000) suggested that $^{40}Ar$ in phengite may represent argon inherited from the protolith of the UHP eclogite, rather than excess, i.e., parentless, argon [nomenclature following McDougall and Harrison (1999)]. Zircon U–Pb ages span a wide range from 210 to 970 Ma with three groups: 210–240 Ma (Ames et al., 1996; Rowley et al., 1997; Hacker et al., 1998; Li et al., 2000; Wan et al., 2005; Xie and Chen, 2005), 420–480 Ma (Jian et al., 1994; Yang et al., 1995; Jian et al., 2000; Gao et al., 2002; Yang et al., 2005) and 650–970 Ma (Liu et al., 1995; Cheng et al., 2000; Wan et al., 2005). A few Early Proterozoic–Late Archean U–Pb ages of 2200–2770 Ma were obtained (Cao and Zhu, 1995, 1996; Liu et al., 1995). Ages for the Bixiling eclogites, the largest outcrop area of mafic eclogites in Dabieshan, have been determined with various isotopic geochronometers. The previous dating results for the Bixiling eclogites are summarized in Table 1. Using a SHRIMP II ion microprobe, Jian and co-workers obtained concordant Caledonian ages of $455 \pm 4$, $452 \pm 3$ and $442 \pm 2$ Ma, respectively, for zircons from the dark coloured eclogite, light coloured eclogite, and granitic gneiss of Bixiling (cited in Yang et al., 2002).

Depending on the dating method, estimates of the age of UHP metamorphism in the Dabie–Sulu terranes range from Triassic, to early Paleozoic, to Neoproterozoic to Neoarchean (see discussion in Yang et al., 2002). Undoubtedly, the last profound metamorphic event occurred in the Triassic with local overprinting by post-tectonic granitoids of Cretaceous age.

### 1.1. Argon isotope systematics of (U)HP metamorphic rocks

The purpose of this study was to investigate Ar isotope systematics of garnet and fluid inclusions in garnet, with the specific aim of studying excess $^{40}Ar$ by the $^{40}Ar/^{39}Ar$ crushing technique given that age scatter attributed to excess $^{40}Ar$ is ubiquitous in the (U)HP metamorphic rocks of Dabieshan (Li et al., 1994), the Seward Peninsula of Alaska (Hannula and McWilliams, 1995), the western Alps (Scaillet et al., 1992; Arnaud and Kelley, 1995; Ruffet et al., 1995, 1997; Scaillet, 1996), the Holsnoy Island of western Norway (Boundy et al., 1997), the Pakistan Himalaya (Tonarini et al., 1993), and the Tavsanli Zone of NW Turkey (Sherlock and Arnaud, 1999; Sherlock and Kelley, 2002).

It should be noted, however, that for some of the samples from the western Alps, Carrapa et al. (2003) argued that anomalously old ages may be a consequence of inherited argon rather than of excess argon, i.e., as vestiges of the pre-metamorphic geologic history of these rocks that survived the last, Eocene–Miocene metamorphic events. Giorgis et al. (2000) made a similar point for the Sulu eclogite phengites. The mobility of $^{40}Ar$ during UHP metamorphism is still poorly understood (Scaillet, 1996, 1998; Sherlock and Arnaud, 1999; Kelley, 2002; Sherlock and Kelley, 2002). No convincing evidence has been obtained, so far, on either the timing of incorporation of excess argon or the processes by which the argon becomes trapped in the lattice of some minerals. Better understanding of the process will help to improve our understanding

Table 1
The previous dating results for the Bixiling eclogites

| Method | Mineral | Age type | Apparent age (Ma) | Reference |
|---|---|---|---|---|
| U–Pb TIMS | Zircon | Upper intersection | 2774 ± 24 | Cao and Zhu (1995, 1996) |
| | | Lower intersection | 452 ± 78 | |
| | | Upper intersection | 2210 ± 39 | Liu et al. (1995) |
| | | Lower intersection | 907 ± 100 | |
| | | Upper intersection | 818 ± 163 | Liu et al. (1995) |
| | | Lower intersection | 247 ± 68 | |
| U–Pb SHRIMP | Zircon core | | 757 ± 7 | Cheng et al. (2000) |
| | Zircon rims | | 223 ± 3 | |
| | Zircon from dark eclogite | | 455 ± 4 Ma | |
| | Zircon from light eclogite | Weighted mean age | 452 ± 3 Ma | P. Jian (cited in Yang et al. (2002)) |
| | Zircon from gneiss | | 442 ± 2 Ma | |
| Sm–Nd | Grt, Omp and WR | Isochron age | 210 ~ 218 | Chavagnac and Jahn (1996) |
| | Seven Grts | Isochron age | 225 ± 7 | |
| Rb–Sr | Phg and (WR, Omp or Grt) | Isochron age | 198 ~ 223 | Chavagnac and Jahn (1996) |
| $^{40}Ar/^{39}Ar$ stepwise heating | Phengite | Plateau age | 528 ± 7 | Wang et al. (2000) |
| | | Isochron age | 517 ± 17 | |
| | Omphacite | Plateau age | 321 ± 5 | Wang et al. (2000) |
| | | Isochron age | 339 ± 15 | |
| $^{40}Ar/^{39}Ar$ laser fusing | Grt, Omp | Isochron age | 400 ± 18 | Hu et al. (1999) |

WR, Whole rock; Phg, Phengite; Omp, Omphacite; Grt, Garnet.

of the thermal evolution of UHP continental crustal rocks.

Our approach in the present study is novel in that it is the first to document the argon isotope systematics of the fluid phase encapsulated in metamorphic minerals. In noble gas geochemistry stepwise crushing is a commonly used technique to distinguish the gas component trapped inside fluid inclusions and on the grain boundaries of solid inclusions from the component of the gas trapped inside the crystal lattice. The latter component subsequently may be liberated by stepwise heating the remaining powder. Since Kelley et al. (1986) attempted to analyze fluid inclusions by the $^{40}Ar/^{39}Ar$ method using crushing gas-extraction technique, it has been demonstrated that fluid inclusions in quartz from hydrothermal deposits can be dated by crushing in vacuum (Turner and Bannon, 1992; Turner and Wang, 1992; Qiu, 1996; Kendrick et al., 2001; Qiu et al., 2002a,b). Concordant $^{40}Ar/^{39}Ar$ ages of quartz hosted fluid inclusions by crushing and those of muscovite and other K-rich micro-crystals by heating have been reported in several studies (Qiu, 1996; Qiu et al., 2002a,b).

In this study, we use the stepwise crushing technique in an attempt to investigate and perhaps date the fluid inclusions in garnets from the Bixiling eclogites in order to shed further light on fluid mobility during UHP metamorphism. Unexpectedly, we obtained very interesting $^{40}Ar/^{39}Ar$ age results with plateau ages and good isochrons by the $^{40}Ar/^{39}Ar$ progressive crushing technique, which form the main focus of the present paper. If an old prograde argon age signal is to be preserved in metamorphic garnet formed at temperatures in excess of 700–800 °C (see below), then the diffusion rate of argon in garnet in the HT metamorphic domain must be very low. We are not aware of any information in the literature on the diffusion rate of argon in garnet. Dunai and Roselieb (1996), however, showed that the closure temperature for helium in garnet could be as high as ca. 630 °C. Given the larger size of the argon atom relative to the helium atom and assuming the same mechanism for diffusion, it follows that the closure temperature for argon diffusion in garnet may be considerably higher than 630 °C. Thus, if the host garnet remains stable during subsequent metamorphic overprinting, it is possible that primary fluid inclusion ages in garnet may survive high temperature metamorphism. The data presented in our work appears to support this notion, which may offer a new approach to dating metamorphic histories in complex metamorphic terrains.

## 2. Petrology and fluid inclusions

The Bixiling mafic-ultramafic metamorphic complex is a 1.5 $km^2$ tectonic block within biotite gneiss in the southern Dabie ultra-high-pressure terrane (Fig. 1). The complex consists of banded felsic and mafic eclogites that contain thin layers of garnet-bearing cumulate ultramafic rock. Detailed petrological and geochemical studies have been made by Zhang et al. (1995). All the eclogite samples in this study are light in colour and rich in kyanite, the same as type (3) of "foliated kyanite-rich, talc-bearing coesite eclogite" described by Zhang et al. (1995) who distinguished six types of eclogites in Bixiling. The light-coloured eclogites contain garnet, omphacite, quartz, kyanite and phengite, along with minor rutile (Fig. 2). Coesite and its pseudomorphs occur as inclusions in garnet and omphacite (Zhang et al., 1995). The minerals show little alteration, deformation or weathering. Zhang et al. (1995) concluded that the ultramafic metamorphic assemblages formed at 700–800 °C and 47–67 kbar, following initial emplacement at

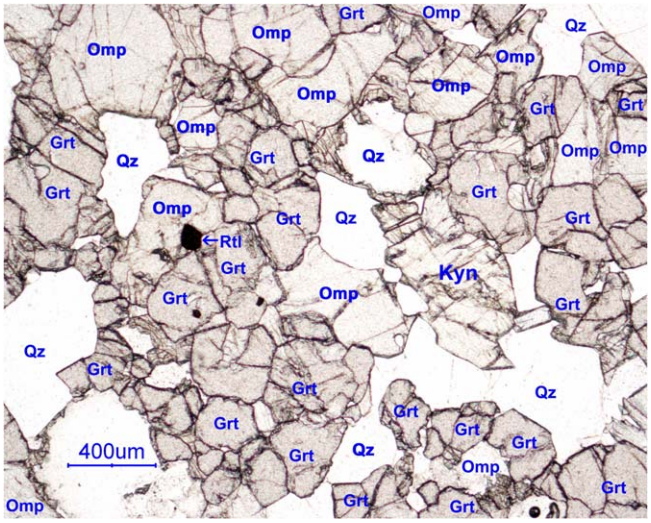


Fig. 2. Photomicrograph showing paragenesis and texture of eclogite DB-1. Grt, Garnet; Omp, Omphacite; Kyn, Kyanite; Rtl, Rutile; Qz, Quartz.

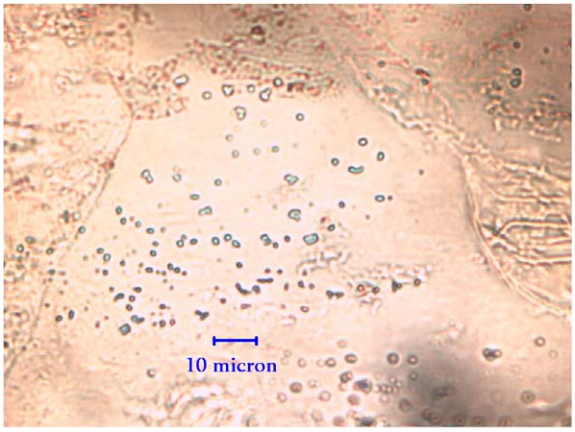


Fig. 3. Photomicrograph showing the primary fluid inclusions in garnet of eclogite DB-1.

normal crustal levels and subsequent subduction to great depths (>100 km) during the collision of the Sino-Korean and Yangtze cratons.

Table 2a
Microprobe analyses of the Bixiling eclogites (Average)

| Sample: | DB-1 | | | | 02BX018 | | | |
|---|---|---|---|---|---|---|---|---|
| Mineral: | Grt | Cpx | Grt | Cpx | Grt | Cpx | Grt | Cpx |
| Spot: | 6 | 6 | 6 | 6 | 3 | 3 | 3 | 3 |
| Positiont: | Core | Core | Rim | Rim | Core | Core | Rim | Rim |
| *(a) Garnets and clinopyroxenes* | | | | | | | | |
| $SiO_2$ | 40.1 | 56.8 | 39.9 | 56.3 | 40.5 | 56.3 | 40.5 | 55.3 |
| $TiO_2$ | 0.03 | 0.04 | 0.01 | 0.05 | 0.03 | 0.02 | 0.00 | 0.03 |
| $Al_2O_3$ | 22.7 | 10.7 | 22.6 | 10.1 | 22.4 | 10.99 | 22.5 | 9.27 |
| $Cr_2O_3$ | 0.02 | 0.06 | 0.01 | 0.02 | 0.01 | 0.03 | 0.00 | 0.01 |
| FeO | 17. 5 | 2.50 | 18.6 | 2.83 | 15.2 | 1.63 | 17.6 | 2.19 |
| MnO | 0.38 | 0.02 | 0.42 | 0.01 | 0.31 | 0.02 | 0.40 | 0.01 |
| MgO | 9.95 | 9.23 | 9.00 | 9.84 | 9.30 | 9.58 | 9.65 | 10.54 |
| CaO | 9.57 | 13.77 | 9.46 | 14.97 | 12.12 | 14.4 | 9.42 | 16.1 |
| SrO | | 0.04 | | 0.02 | | 0.04 | | 0.03 |
| $Na_2O$ | 0.03 | 6.75 | 0.04 | 6.06 | 0.03 | 6.21 | 0.01 | 5.25 |
| Total | 100.2 | 99.9 | 100.1 | 100.2 | 99.9 | 99.3 | 100.0 | 98.7 |
| Si | 3.00 | 2.01 | 3.01 | 1.99 | 3.03 | 2.00 | 3.04 | 1.99 |
| Ti | 0.00 | 0.00 | 0.00 | 0.00 | 0.00 | 0.00 | 0.00 | 0.00 |
| Al | 2.00 | 0.45 | 2.00 | 0.42 | 1.98 | 0.46 | 1.99 | 0.39 |
| Cr | 0.00 | 0.00 | 0.00 | 0.00 | 0.00 | 0.00 | 0.00 | 0.00 |
| Fe | 1.09 | 0.07 | 1.17 | 0.08 | 0.95 | 0.05 | 1.10 | 0.07 |
| Mn | 0.02 | 0.00 | 0.03 | 0.00 | 0.02 | 0.00 | 0.03 | 0.00 |
| Mg | 1.11 | 0.49 | 1.01 | 0.52 | 1.04 | 0.51 | 1.08 | 0.57 |
| Ca | 0.77 | 0.52 | 0.76 | 0.57 | 0.97 | 0.55 | 0.76 | 0.62 |
| Sr | | 0.00 | | 0.00 | | 0.00 | | 0.00 |
| Na | 0.00 | 0.46 | 0.01 | 0.42 | 0.00 | 0.43 | 0.00 | 0.37 |
| Cations | 8.0 | 4.00 | 8.0 | 4.00 | 8.00 | 4.00 | 8.00 | 4.00 |
| Charge | 24.0 | 12.00 | 24.0 | 11.99 | 24.0 | 12.0 | 24.1 | 12.0 |
| $Fe^{3+}$_calc | 0.01 | 0.00 | 0.01 | 0.01 | −0.04 | −0.04 | −0.07 | −0.01 |
| $Fe^{2+}$_calc | 1.08 | 0.07 | 1.17 | 0.07 | 0.99 | 0.09 | 1.17 | 0.08 |
| Total_calc | 100.2 | 99.9 | 100.1 | 100.2 | 99.9 | 99.1 | 99.8 | 98.6 |
| $K_D$ | 6.82 | | 8.34 | | 9.80 | | 9.04 | |
| $X_{Ca}^{GT}$ | 0.26 | | 0.26 | | 0.33 | | 0.26 | |
| $T_{PW}$ (°C) | 790 | | 735 | | 748 | | 714 | |
| $T_{KR}$ (°C) | 783 | | 723 | | 739 | | 700 | |
| $T_{EG}$ (°C) | 812 | | 757 | | 769 | | 736 | |

*T* (°C) at 30 kbar. KR, Krogh (1988). PW, Powell (1985). EG, Ellis and Green (1979).

Table 2b
Microprobe analyses of the Bixiling eclogites (Average)

| Sample: | 02BX018 | DB-4 | DB-6 |
|---|---|---|---|
| Spot: | 10 | 4 | 2 |
| *(b) Phengites* | | | |
| $SiO_2$ | 53.2 | 49.4 | 51.0 |
| $TiO_2$ | 0.22 | 0.55 | 0.37 |
| $Al_2O_3$ | 26.9 | 26.5 | 24.7 |
| FeO | 1.03 | 2.52 | 2.70 |
| MnO | 0.01 | 0.00 | 0.01 |
| MgO | 4.04 | 3.40 | 4.02 |
| CaO | 0.02 | 0.00 | 0.06 |
| SrO | 0.03 | 0.05 | 0.02 |
| $Na_2O$ | 0.40 | 0.65 | 0.24 |
| $K_2O$ | 10.15 | 10.25 | 10.75 |
| BaO | 0.36 | | |
| F | 0.03 | 0.04 | 0.02 |
| Cl | 0.01 | 0.01 | 0.00 |
| O_F_Cl | 0.01 | 0.02 | 0.01 |
| Total | 96.4 | 93.4 | 93.8 |
| $H_2O$_calc | 4.57 | 4.37 | 4.40 |
| Total_calc | 101.0 | 97.7 | 98.2 |
| Si | 6.95 | 6.75 | 6.94 |
| Ti | 0.02 | 0.06 | 0.04 |
| Al | 4.15 | 4.28 | 3.97 |
| Fe | 0.11 | 0.29 | 0.31 |
| Mn | 0.00 | 0.00 | 0.00 |
| Mg | 0.79 | 0.69 | 0.81 |
| Ca | 0.00 | 0.00 | 0.01 |
| Sr | 0.00 | 0.00 | 0.00 |
| K | 1.69 | 1.79 | 1.87 |
| Na | 0.10 | 0.17 | 0.07 |
| Ba | 0.02 | | |
| Cations | 13.8 | 14.0 | 14.0 |
| $OH^-$_calc | 3.99 | 3.98 | 4.00 |
| $(Si/Al)_{oct}$ | 6.95 | 5.47 | 7.36 |

$(Si/Al)_{oct}$: the Si/Al ratio in octahedral sites.

The samples in this study were from a newly exposed outcrop in the eastern part of Bixiling, east of Qianshui River (Fig. 1). Compositional data on phengites, garnets, pyroxenes from the eclogites, carried out on a JEOL JXA-8800 M® Electronprobe Microanalyzer at the Faculty of Earth and Life Sciences, Vrije Universiteit Amsterdam, are listed in Table 2a. The temperatures obtained by the garnet-clinopyroxene Fe–Mg exchange thermometer (Ellis and Green, 1979) indicate that the eclogites used for our studies formed in the range 730 (rim) to 820 °C (core) (calculated at $P = 30$ kbar), which are similar to temperatures obtained in previous studies using the same thermometer (Zhang et al., 1995; Xiao et al., 2000) and by oxygen isotope geothermometers (Xiao et al., 2000). All the white mica grains from the Bixiling eclogites are phengites because of their high Si/Al ratios of 3.81–9.96 with an average of 6.63, much higher than 3, in octahedral sites (Table 2b). These high Si compositions are consistent with the interpretation that phengite also formed during UHP metamorphism.

The fluid phase involved in UHP metamorphism of the Dabie eclogites at Bixiling and elsewhere was investigated in several previous studies (Xiao et al., 2000; Fu et al., 2001, 2002, 2003). Five types of fluid inclusions within Bixiling eclogite were distinguished (Xiao et al., 2000): (1) primary Ca-rich brines in quartz blebs in kyanite; (2) primary NaCl-dominated high-salinity inclusions in omphacite and kyanite; (3) primary NaCl-dominated medium- to high-salinity inclusions in matrix quartz; (4) carbonic inclusions in omphacite and matrix quartz; (5) secondary low-salinity aqueous (or pure water) inclusions in matrix quartz. Clusters of water molecules in the elongated garnets of Bixiling were discovered, which indicated the protoliths were able to carry water into the mantle during the subduction of continental lithosphere (Su et al., 2002).

Most of the fluid inclusions in the garnets of Bixiling are primary and small ($\leqslant 3$ μm) (Fig. 3). Their small size in combination with the high refractive index of garnet prevents the determination of their homogenization/freezing temperatures and chemical compositions using a conventional heating–freezing stage. Fluid inclusions in quartz, often much bigger than those in garnet and some of them containing gas bubbles, are distributed within tracks, which may indicate that they are secondary and formed later than those in garnet. Clearly secondary fluid inclusions distributed along micro-cracks in quartz were also observed. In summary, fluids were mobile in the rock during various stages of the metamorphic evolution. It could be argued, therefore, that at least two periods of fluids affected the garnet after its crystallization in terms of the observations of the fluid inclusions in quartz.

## 3. Experimental techniques

Argon isotope ratios were measured on an MAP-215-50 mass spectrometer in the Argon Isotope Laboratory of the Vrije Universiteit Amsterdam using techniques modified from those described by Wijbrans et al. (1995). Samples and monitor standard DRA1 (sanidine with age of $25.26 \pm 0.07$ Ma) were irradiated at the Petten HFR reactor using the Cd-lined RODEO pool-side facility for 18 h. Correction factors for interfering argon isotopes derived from Ca are determined by Wijbrans et al. (1995), the correction factor for K-derived nucleogenic $^{40}Ar$ was re-determined when the Cd-lined tube on Rodeo became operational. The correction factors are: $(^{39}Ar/^{37}Ar)_{Ca} = 6.73 \times 10^{-4}$, $(^{36}Ar/^{37}Ar)_{Ca} = 2.64 \times 10^{-4}$, $(^{40}Ar/^{39}Ar)_K = 1.83 \times 10^{-3}$ and $(^{38}Ar/^{39}Ar)_K = 1.211 \times 10^{-2}$.

In order to obtain $J$-values for the samples, the monitor DRA1 was packed between every five samples in quartz sample tubes, each tube containing 10 to 15 packets of DRA1. From each packet containing DRA1 five splits were used to measure the $J$-values, then taking the weighted mean as the $J$-value. DRA1 is very homogeneous and replication is usually excellent (Wijbrans et al., 1995). Based on the $J$-values and the positions of DRA1 in the sample tube, a regression line of each sample tube was obtained, and then the $J$-values of the samples were calculated

by interpolation from the regression line. The *J*-value uncertainty of 0.15% ($1\sigma$) was propagated into the age calculations.

The crushing experiments were carried out in an in-house designed crushing apparatus which was connected to the extraction line. The crusher consists of a 40 cm long, 4 cm diameter Inconel® tube. The tube has spherical curvature on the inside base. The base is made of a 10 cm long — 4 cm diameter solid rod of Inconel® that was welded to the tube. Crushing is achieved by moving a magnet steel dead-weight, with a machined spherical curvature on the one end, grooves on the side and a threaded nipple on the top end (for easy removal). The curvature on the dead-weight is of slightly smaller radius when compared to that of the crusher base, allowing concentration of powder near the tube central axis during crushing. Prior to analysis, blanks were reduced by heating the whole apparatus to 150 °C using heating tape and the sample tube to 300 °C using a furnace for ca. 12 h. The samples were crushed by repeatedly lifting and dropping the pestle using an external electromagnet with a frequency of one time per second (1 Hz) controlled by an adjustable power supply and pulse generator. The pestle was dropped from a height of 3 to 5 cm. As it was found that the gas yield decreased during the experiment, the number of the pestle movements for each successive extraction step was increased to maintain the argon concentration levels high enough for measurement.

The phengite was analysed using standard single grain laser incremental heating techniques where the laser power is increased for each subsequent step (e.g., Wijbrans et al., 1995). The released gases were purified by a Fe/V/Zr getter pump operated at 250 °C and a Zr/Al pump operated at 450 °C. The purified gas was then analysed for the argon isotopes in the mass spectrometer.

We ran aliquots of air to check the mass spectrometer state at the beginning of experiments. In order to exclude the blank contributions of the line, a blank was run after every three or four gas extraction steps. The blank values are variable but usually blanks on $^{40}Ar$ were 100–1000 times smaller than the amount of gas derived from the crushing experiments. Units used for tabulation of beam intensity data are Volts. Recent calibration using weighed amounts of HdB1 biotite standard ($3.364 \times 10^{-10}$ mol/g radiogenic $^{40}Ar$ content (Lippolt and Hess, 1994) yielded an average value of $7.2 \times 10^{-15}$ moles Ar per Volt for our mass spectrometer.

## 4. Results

The $^{40}Ar/^{39}Ar$ dating results of three garnets DB-1G, 02BX005 and 02BX019 by crushing and a phengite DB-1MS by laser heating are shown in Table 3, and the age spectrum and isochron plots for each sample are shown in Figs. 4–7. The $^{40}Ar/^{39}Ar$ dating results are calculated using the ArArCALC software package (http://earthref.org/tools/ararcalc/index.html) (Koppers, 2002) which consists of Visual Basic® routines that operate as "add-ins" in Microsoft Excel®.

Crushing in vacuum is the accepted technique to release selectively gas trapped in crystalline material in fluid inclusions and along cracks and cavities in the crystal. Crushing apparently has very little effect on the gas component that is trapped within the crystal lattice: the crushing experiment on the Methuen muscovite (Dunlap and Kronenberg, 2001) showed that only ~0.53% of total $^{39}Ar$ was released by crushing. Qiu et al. (2002a) indicated that "strong differences between the results of the crushing and heating experiments of two samples imply that the gases released by crushing were mainly from the fluid inclusions and those by heating were from the mineral component of the samples, which was supported by microscopic observations of the thin sections and the results of EPMA and XRD analyses" and "the gases within the structures of the solid minerals are hardly released by crushing." Therefore, the results obtained from our garnet samples by crushing may be interpreted with some confidence as the contribution of the fluid inclusions trapped inside the crystalline mass. In Section 5, we will argue the validity of this assumption from comparison of the $^{40}Ar/^{39}Ar$ results of garnets with those of phengite.

### 4.1. Garnet DB-1G, 02BX005G and 02BX019G

The $^{40}Ar/^{39}Ar$ ratios of garnet DB-1G as determined from progressive crushing experiments form an age spectrum (Fig. 4a) with apparent ages decreasing dramatically in the first 9 steps and then an age plateau appears from steps 10–22 corresponding to a plateau age of $427 \pm 20$ Ma (taking about 59.5% of the total $^{39}Ar$ released by crushing) by correcting the non-radiogenic $^{40}Ar$ using the $^{40}Ar/^{36}Ar$ ratio of the modern atmosphere (295.5). On the inverse isochron diagram of $^{36}Ar/^{40}Ar$ vs $^{39}Ar/^{40}Ar$, a well-defined isochron is obtained from the data points of stages 10 to 22 which corresponds to an isochron age of $448 \pm 34$ Ma, an initial $^{40}Ar/^{36}Ar$ ratio of $292 \pm 5$ and an MSWD = 4.1 (Fig. 4b). This initial $^{40}Ar/^{36}Ar$ ratio is within error of that determined for present-day atmosphere. A plateau age of $449 \pm 18$ Ma is obtained when applying this ratio to correct the non-radiogenic $^{40}Ar$ (Fig. 4a), which is in agreement with its isochron age, indicating the time when the primary fluid inclusions were trapped and therefore the garnet formed ca. 450 Ma ago.

The $^{40}Ar/^{39}Ar$ dating results of garnets 02BX005G and 02BX019G by crushing in vacuo also form quite similar age spectra and isochron diagrams (Figs. 5 and 6) to those of the garnet DB-1G: (1) Both age spectra show a decrease in apparent ages in the beginning steps, and these apparent ages are all much higher than expected, which indicates that excess $^{40}Ar$ exists within the bigger, easily crushed, secondary fluid inclusions. (2) Both garnets reveal age plateaux in the final steps with concordant plateau ages of $450 \pm 31$ and $449 \pm 10$ Ma, respectively (when applying

Table 3
$^{40}Ar/^{39}Ar$ dating results

| Step | Pestle drop numbers | $^{36}Ar_A$ | $^{37}Ar_{Ca}$ | $^{38}Ar_{Cl}$ | $^{39}Ar_K$ | $^{40}Ar^*$ | Age $\pm 2\sigma$ (Ma) | $^{40}Ar^*$ (%) | $^{39}Ar_K$ (%) |
|---|---|---|---|---|---|---|---|---|---|
| *(a) Garnet DB-1G by crushing in vacuum, J = 0.004707, wt = 0.03500 g* | | | | | | | | | |
| 1[a] | 8 | 0.02051 | 0.32774 | 0.01113 | 0.03250 | 11.69307 | 1787.4 ± 21.2 | 65.86 | 8.48 |
| 2[a] | 10 | 0.00911 | 0.11076 | 0.00018 | 0.00971 | 4.94388 | 2206.4 ± 64.3 | 64.75 | 2.53 |
| 3[a] | 15 | 0.00489 | 0.11089 | 0.00021 | 0.00669 | 3.45820 | 2226.0 ± 84.6 | 70.54 | 1.74 |
| 4[a] | 20 | 0.00610 | 0.11499 | 0.00026 | 0.00996 | 2.88139 | 1549.9 ± 55.3 | 61.53 | 2.60 |
| 5[a] | 30 | 0.00690 | 0.15286 | 0.00006 | 0.01130 | 3.79320 | 1709.9 ± 56.0 | 65.05 | 2.95 |
| 6[a] | 45 | 0.01037 | 0.33253 | 0.00019 | 0.01712 | 5.48263 | 1658.2 ± 41.0 | 64.15 | 4.46 |
| 7[a] | 60 | 0.01368 | 0.36985 | 0.00008 | 0.02007 | 2.49814 | 831.9 ± 33.7 | 38.19 | 5.23 |
| 8[a] | 80 | 0.01382 | 0.50270 | 0.00003 | 0.02276 | 3.06295 | 885.3 ± 15.0 | 42.87 | 5.93 |
| 9[a] | 100 | 0.01713 | 0.60414 | 0.00029 | 0.02534 | 2.78876 | 752.9 ± 24.0 | 35.52 | 6.61 |
| 10 | 130 | 0.01873 | 0.83619 | 0.00025 | 0.02897 | 1.67318 | 433.9 ± 11.2 | 23.21 | 7.55 |
| 11 | 160 | 0.05352 | 1.10641 | 0.00016 | 0.03074 | 1.80648 | 440.5 ± 54.9 | 10.25 | 8.02 |
| 12 | 160 | 0.02084 | 1.03891 | 0.00028 | 0.02627 | 1.35682 | 392.6 ± 41.2 | 18.05 | 6.85 |
| 13 | 190 | 0.02592 | 1.06574 | 0.00029 | 0.02696 | 1.71723 | 473.0 ± 31.8 | 18.31 | 7.03 |
| 14 | 210 | 0.02879 | 1.23637 | 0.00051 | 0.02223 | 1.03150 | 356.4 ± 57.0 | 10.82 | 5.80 |
| 15 | 210 | 0.02882 | 1.07870 | 0.00000 | 0.01525 | 0.53874 | 277.5 ± 79.5 | 5.95 | 3.98 |
| 16 | 210 | 0.03512 | 0.96436 | 0.00014 | 0.01012 | 0.37044 | 286.8 ± 129.0 | 3.45 | 2.64 |
| 17 | 210 | 0.02584 | 0.86191 | 0.00041 | 0.00874 | 0.69210 | 571.7 ± 135.6 | 8.31 | 2.28 |
| 18 | 230 | 0.02925 | 1.12377 | 0.00049 | 0.01180 | 0.60794 | 391.8 ± 131.6 | 6.57 | 3.08 |
| 19 | 240 | 0.02700 | 1.09478 | 0.00031 | 0.01168 | 0.66270 | 427.1 ± 104.7 | 7.67 | 3.05 |
| 20 | 250 | 0.02574 | 1.14535 | 0.00030 | 0.01100 | 0.54879 | 380.4 ± 48.7 | 6.73 | 2.87 |
| 21 | 280 | 0.03120 | 1.25977 | 0.00063 | 0.01250 | 0.79675 | 473.4 ± 70.2 | 7.96 | 3.26 |
| 22 | 300 | 0.03757 | 1.31765 | 0.00044 | 0.01177 | 0.53106 | 347.4 ± 70.1 | 4.57 | 3.07 |
| *(b) Garnet 02BX005G by crushing, J = 0.002015, wt = 0.03204 g* | | | | | | | | | |
| 1[a] | 100 | 0.06301 | 0.80906 | 0.00000 | 0.02302 | 71.76545 | 3581.8 ± 41.8 | 79.40 | 15.93 |
| 2[a] | 100 | 0.01365 | 0.32720 | 0.00057 | 0.00626 | 9.65042 | 2548.8 ± 84.8 | 70.52 | 4.33 |
| 3[a] | 250 | 0.02809 | 1.04989 | 0.00067 | 0.01783 | 20.69621 | 2175.2 ± 47.7 | 71.37 | 12.34 |
| 4[a] | 360 | 0.03155 | 1.06498 | 0.00146 | 0.01539 | 17.33187 | 2137.2 ± 29.8 | 65.02 | 10.65 |
| 5[a] | 540 | 0.02331 | 1.35027 | 0.00000 | 0.01471 | 16.48185 | 2130.9 ± 116.7 | 70.53 | 10.18 |
| 6[a] | 540 | 0.01574 | 0.97905 | 0.00000 | 0.00787 | 6.95928 | 1845.6 ± 177.9 | 59.93 | 5.45 |
| 7[a] | 540 | 0.01612 | 0.93491 | 0.00000 | 0.00722 | 5.07913 | 1592.9 ± 188.4 | 51.60 | 4.99 |
| 8[a] | 540 | 0.02501 | 0.75979 | 0.00000 | 0.00534 | 2.54236 | 1213.4 ± 223.1 | 25.60 | 3.70 |
| 9[a] | 540 | 0.01005 | 0.67637 | 0.00000 | 0.00479 | 1.36567 | 818.4 ± 162.0 | 31.50 | 3.32 |
| 10[a] | 540 | 0.01117 | 0.53113 | 0.00000 | 0.00285 | 0.95198 | 928.1 ± 328.4 | 22.39 | 1.97 |
| 11[a] | 540 | 0.01100 | 0.45549 | 0.00000 | 0.00207 | 0.61427 | 846.1 ± 416.6 | 15.90 | 1.43 |
| 12 | 450 | 0.00615 | 0.36297 | 0.00058 | 0.00384 | 0.63343 | 518.2 ± 52.5 | 25.86 | 2.65 |
| 13 | 450 | 0.02787 | 0.31782 | 0.00084 | 0.00333 | 0.45846 | 441.7 ± 97.7 | 5.27 | 2.30 |
| 14 | 450 | 0.00689 | 0.32307 | 0.00129 | 0.00264 | 0.41647 | 498.5 ± 110.4 | 16.99 | 1.82 |
| 15 | 450 | 0.00435 | 0.26646 | 0.00115 | 0.00283 | 0.38522 | 437.6 ± 94.3 | 23.06 | 1.96 |
| 16 | 540 | 0.00658 | 0.31933 | 0.00114 | 0.00330 | 0.40274 | 396.6 ± 64.2 | 17.16 | 2.28 |
| 17 | 540 | 0.00855 | 0.30528 | 0.00108 | 0.00245 | 0.30428 | 403.0 ± 80.1 | 10.75 | 1.69 |
| 18 | 540 | 0.01030 | 0.29333 | 0.00113 | 0.00186 | 0.29748 | 504.9 ± 145.7 | 8.90 | 1.28 |
| 19 | 540 | 0.00562 | 0.30840 | 0.00188 | 0.00362 | 0.43673 | 392.6 ± 99.9 | 20.81 | 2.50 |
| 20 | 540 | 0.00531 | 0.31823 | 0.00197 | 0.00280 | 0.46591 | 521.2 ± 105.1 | 22.91 | 1.94 |
| 21 | 630 | 0.00563 | 0.35372 | 0.00321 | 0.00436 | 0.53061 | 395.8 ± 71.9 | 24.19 | 3.02 |
| 22 | 630 | 0.00968 | 0.29725 | 0.00313 | 0.00272 | 0.37411 | 440.7 ± 93.4 | 11.57 | 1.89 |
| 23 | 630 | 0.00777 | 0.33874 | 0.00326 | 0.00344 | 0.43162 | 407.0 ± 82.6 | 15.83 | 2.38 |
| *(c) Garnet 02BX019G by crushing, J = 0.002009, wt = 0.03995 g* | | | | | | | | | |
| 1[a] | 150 | 0.04740 | 0.42108 | 0.00074 | 0.02169 | 21.58763 | 1981.8 ± 22.12 | 60.65 | 5.81 |
| 2[a] | 270 | 0.03660 | 0.59102 | 0.00063 | 0.02535 | 10.02876 | 1055.3 ± 17.13 | 48.11 | 6.79 |
| 3[a] | 360 | 0.04845 | 0.83005 | 0.00131 | 0.03481 | 9.32054 | 776.6 ± 14.68 | 39.43 | 9.32 |
| 4[a] | 450 | 0.05005 | 0.94362 | 0.00124 | 0.03844 | 8.44792 | 659.8 ± 12.66 | 36.35 | 10.29 |
| 5[a] | 450 | 0.05098 | 0.67791 | 0.00081 | 0.02710 | 6.22333 | 684.3 ± 13.39 | 29.24 | 7.26 |
| 6[a] | 450 | 0.07750 | 0.48317 | 0.00061 | 0.01684 | 3.56975 | 640.0 ± 33.19 | 13.49 | 4.51 |
| 7[a] | 450 | 0.01935 | 0.37733 | 0.00038 | 0.01246 | 1.96181 | 495.7 ± 22.45 | 25.55 | 3.34 |
| 8[a] | 450 | 0.01404 | 0.33323 | 0.00052 | 0.00873 | 1.36383 | 492.3 ± 27.43 | 24.74 | 2.34 |
| 9[a] | 450 | 0.01265 | 0.34493 | 0.00157 | 0.00833 | 1.32119 | 499.0 ± 26.0 | 26.11 | 2.23 |
| 10[a] | 450 | 0.01233 | 0.25015 | 0.00064 | 0.00872 | 1.37262 | 495.7 ± 32.1 | 27.37 | 2.34 |
| 11[a] | 450 | 0.01557 | 0.40263 | 0.00168 | 0.01684 | 3.21513 | 585.6 ± 23.2 | 41.14 | 4.51 |
| 12[a] | 450 | 0.01129 | 0.38702 | 0.00136 | 0.01781 | 2.90071 | 510.7 ± 15.3 | 46.52 | 4.77 |
| 13[a] | 540 | 0.01258 | 0.50378 | 0.00109 | 0.02271 | 3.80621 | 523.6 ± 14.3 | 50.60 | 6.08 |
| 14 | 540 | 0.00995 | 0.41429 | 0.00103 | 0.01615 | 2.34847 | 462.3 ± 22.4 | 44.40 | 4.33 |

Table 3 (*continued*)

| Step | Pestle drop numbers | $^{36}Ar_A$ | $^{37}Ar_{Ca}$ | $^{38}Ar_{Cl}$ | $^{39}Ar_K$ | $^{40}Ar^*$ | Age $\pm 2\sigma$ (Ma) | $^{40}Ar^*$ (%) | $^{39}Ar_K$ (%) |
|---|---|---|---|---|---|---|---|---|---|
| 15 | 540 | 0.01287 | 0.47995 | 0.00071 | 0.01785 | 2.52624 | 451.5 ± 17.5 | 39.92 | 4.78 |
| 16 | 540 | 0.01114 | 0.42407 | 0.00000 | 0.01544 | 2.09985 | 435.7 ± 20.2 | 38.94 | 4.14 |
| 17 | 540 | 0.01121 | 0.45696 | 0.00105 | 0.01400 | 1.96597 | 448.4 ± 19.0 | 37.23 | 3.75 |
| 18 | 540 | 0.01959 | 0.42238 | 0.00038 | 0.00962 | 1.26246 | 422.1 ± 29.9 | 17.90 | 2.58 |
| 19 | 540 | 0.01530 | 0.49893 | 0.00112 | 0.01353 | 1.75648 | 418.2 ± 21.2 | 27.98 | 3.62 |
| 20 | 540 | 0.01950 | 0.37054 | 0.00051 | 0.00670 | 0.87452 | 420.2 ± 47.9 | 13.18 | 1.79 |
| 21 | 540 | 0.00951 | 0.29969 | 0.00024 | 0.00312 | 0.46308 | 470.7 ± 71.9 | 14.14 | 0.84 |
| 22 | 630 | 0.00987 | 0.38211 | 0.00059 | 0.00422 | 0.57510 | 436.9 ± 71.0 | 16.48 | 1.13 |
| 23 | 720 | 0.02474 | 0.78862 | 0.00111 | 0.01298 | 1.85798 | 455.9 ± 17.9 | 20.26 | 3.48 |
| *(d) Phengite DB-1MS by laser stepped heating, J = 0.004784* | | | | | | | | | |
| Step | *Laser powers* | $^{36}Ar_A$ | $^{37}Ar_{Ca}$ | $^{38}Ar_{Cl}$ | $^{39}Ar_K$ | $^{40}Ar^*$ | Age (Ma) $\pm 2\sigma$ | $^{40}Ar^*$ (%) | $^{39}Ar_K$ (%) |
| 1[a] | 0.15 W | 0.00105 | 0.00000 | 0.00000 | 0.01444 | 1.30180 | 646.8 ± 48.0 | 80.81 | 0.47 |
| 2 | 0.25 W | 0.00196 | 0.00000 | 0.00000 | 0.05740 | 5.40949 | 671.4 ± 13.8 | 90.35 | 1.86 |
| 3 | 0.30 W | 0.00115 | 0.00000 | 0.00020 | 0.06319 | 5.46312 | 624.5 ± 16.8 | 94.15 | 2.04 |
| 4[a] | 0.35 W | 0.00219 | 0.03300 | 0.00034 | 0.19993 | 13.40358 | 501.9 ± 5.7 | 95.39 | 6.46 |
| 5 | 0.38 W | 0.00339 | 0.00068 | 0.00017 | 0.35132 | 26.32682 | 552.7 ± 3.6 | 96.33 | 11.36 |
| 6 | 0.41 W | 0.00258 | 0.05011 | 0.00007 | 0.30335 | 22.46300 | 547.1 ± 2.3 | 96.72 | 9.81 |
| 7 | 0.45 W | 0.00462 | 0.00000 | 0.00027 | 0.39498 | 35.93599 | 651.9 ± 4.1 | 96.34 | 12.77 |
| 8 | 0.50 W | 0.00299 | 0.00000 | 0.00000 | 0.19062 | 18.19797 | 678.7 ± 3.3 | 95.36 | 6.16 |
| 9 | 0.55 W | 0.00184 | 0.02412 | 0.00000 | 0.12638 | 11.16373 | 635.9 ± 3.7 | 95.36 | 4.08 |
| 10 | 0.62 W | 0.00093 | 0.04381 | 0.00006 | 0.06081 | 4.96927 | 595.3 ± 7.2 | 94.78 | 1.97 |
| 11 | 0.70 W | 0.00064 | 0.02521 | 0.00028 | 0.08196 | 6.04376 | 545.1 ± 7.0 | 96.95 | 2.65 |
| 12 | 0.80 W | 0.00517 | 0.00000 | 0.00000 | 0.65292 | 46.66818 | 530.6 ± 2.2 | 96.83 | 21.10 |
| 13[a] | 0.85 W | 0.00069 | 0.00202 | 0.00049 | 0.06663 | 4.25842 | 481.3 ± 9.2 | 95.42 | 2.15 |
| 14 | 0.90 W | 0.00017 | 0.00000 | 0.00063 | 0.01826 | 1.32901 | 539.0 ± 37.0 | 96.44 | 0.59 |
| 15 | Fused | 0.00409 | 0.00000 | 0.00014 | 0.51159 | 40.04485 | 573.8 ± 2.2 | 97.07 | 16.54 |

The argon isotopes are listed in volt.

[a] Steps excluded from the isochron age calculations.

their initial $^{40}Ar/^{36}Ar$ ratios from the isochron lines to exclude the non-radiogenic $^{40}Ar$). (3) The data points of the steps contributing to the plateaux yield isochron lines with concordant isochron ages of 459 ± 58 and 450 ± 22 Ma corresponding to initial $^{40}Ar/^{36}Ar$ ratios of 294.5 ± 6.7 and 293.9 ± 5.8, respectively, which also indicates that no excess $^{40}Ar$ is present within the small primary fluid inclusions.

In summary, all three garnets yielded similar age spectra, similar initial $^{40}Ar/^{36}Ar$ ratios and plateau ages pointing to formation during the Caledonian period.

### 4.2. Phengite DB-1MS

The phengite of sample DB-1MS analyzed by laser stepped heating yielded a complicated two-saddle-shaped age spectrum with a total fusion age of 575 ± 3 Ma (Fig. 7a).

In the isotope correlation diagram of $^{36}Ar/^{40}Ar$–$^{39}Ar/^{40}Ar$ based on the $^{40}Ar/^{39}Ar$ dating results, the points show an isochron trend but scatter significantly. An isochron age of 463 ± 116 Ma with an initial $^{40}Ar/^{36}Ar$ ratio of 1843 ± 1740 is obtained by excluding three points (blank square) far removed from the isochron line (Fig. 7b). Applying this initial ratio to correct the non-radiogenic $^{40}Ar$ component, a spectrum corresponding to a lower age for each step is obtained with a total fusion age of 468 ± 6 Ma (the dotted lines in Fig. 7a).

## 5. Discussion

### 5.1. Garnet age spectra

The proportions of $^{39}Ar$ defining the age plateaux of the three garnets show that DB-1G was less profoundly affected by secondary fluids than 02BX005G and 02BX019G. The key $^{40}Ar/^{39}Ar$ data obtained from the crushing experiments on the three garnets are listed in Table 4. The isochron and plateau ages of the three garnets are concordant, which suggests that they are geologically meaningful.

Comparing these new results with the $^{40}Ar/^{39}Ar$ dating results of crushed quartz samples from hydrothermal deposits that contain excess $^{40}Ar$ within fluid inclusions (Qiu, 1996; Qiu et al., 2002a,b), we note that the shapes of the spectra have features in common. Both types of experiments show spectra with very high initial ages that decrease towards a plateau in the final 25–33% of the gas release. However, the distributions of the data points in the isochron diagrams are quite different. In the case of the hydrothermal quartz samples all the points are typically distributed near the isochron lines with high initial $^{40}Ar/^{36}Ar$ ratios showing clearly the presence of excess $^{40}Ar$ within all fluid inclusions. The argon isotope correlation diagrams show contributions from two reservoirs: (1) radiogenic $^{40}Ar$ formed by the decay of $^{40}K$ within the fluid inclusions and (2) the initial Ar component trapped in the

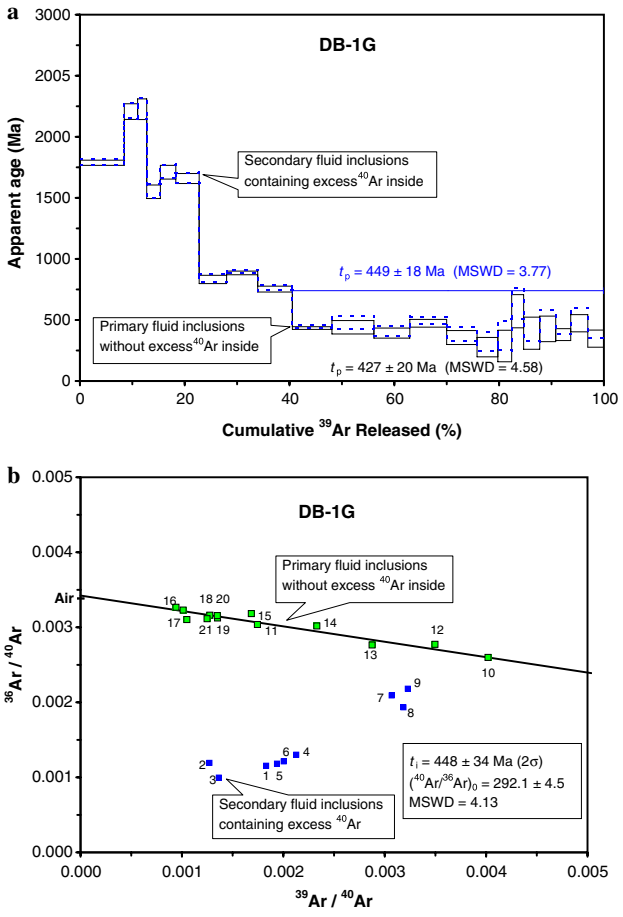


Fig. 4. $^{40}Ar/^{39}Ar$ dating results of garnet DB-1G by crushing: (a) age spectra; (b) inverse isochron. The apparent ages marked by solid and dot lines are calculated, respectively by applying modern atmosphere $^{40}Ar/^{36}Ar$ ratio 295.5 and the initial $^{40}Ar/^{36}Ar$ ratios from the isochron plot to correct the non-radiogenic $^{40}Ar$.

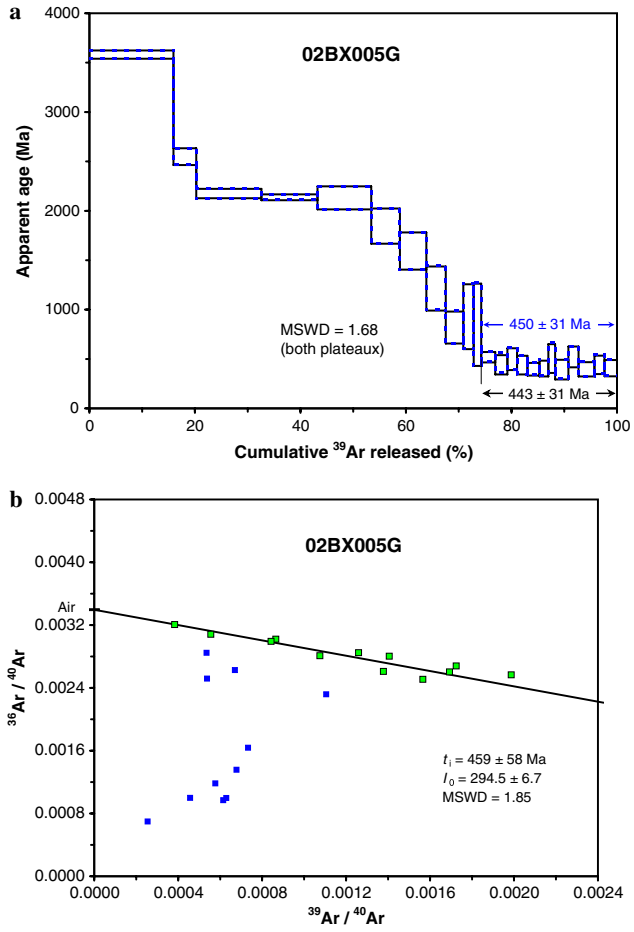


Fig. 5. $^{40}Ar/^{39}Ar$ dating results of garnet 02BX005G by crushing: (a) age spectra; (b) inverse isochron.

fluids. This two sources of argon form a simple two reservoir mixing line. In contrast, for garnets DB-1G, 02BX005G and 02BX019G, we observe a clear division into two separate populations of points. The first group is characterized by easily liberated gas with an argon isotope composition that shows a scattered distribution in the isochron diagram and yields anomalously old ages in the age spectrum. This group shows a typical excess argon trend but no linear array, suggestive of mixing of at least three components. The second group comprises gas that is only released after prolonged crushing and that is characterized by a well-defined isochron with a non-radiogenic intercept close to modern atmosphere. From these results we conclude that the argon isotopic signal obtained from the fluid inclusions of these garnets can be explained in terms of three reservoirs contributing to the observed argon release. The first reservoir contributes mainly excess $^{40}Ar$ to the initial steps of the experiment, the second contributes an Early Paleozoic radiogenic signal and the third contributes an atmospheric signal. The radiogenic and atmospheric argon components form well-defined isochrons. As the release of these two components is apparently linked, we assume that they are derived from the same source. One possibility is that excess argon is so much more abundant in the first steps of the experiments that it may hide the contribution of radiogenic and atmospheric argon. More likely, the excess argon resides in a different class of inclusions that is not linked to the source of the radiogenic and atmospheric argon.

We assume that in stepwise crushing experiments the largest, most easily crushed inclusions contribute to the gas in the initial steps of the experiment. We base this assumption on the observation that during this stage of the experiment, large gas intensities are generated by limited crushing movements (1–10 impacts per step). This gas fraction is dominated by excess $^{40}Ar$ which we argue is hosted in the larger secondary inclusions, most likely incorporated into the garnet during a phase of increased fluid mobility after the peak UHP conditions or even later, after UHP metamorphism had ended. High concentrations of excess $^{40}Ar$ at the grain boundaries are commonly attributed to the effects of cumulative release of radiogenic $^{40}Ar$ from the protolith that degassed during metamorphism (e.g., Kelley, 2002). Once released from the crystalline reservoir it was dissolved in the fluid phase that was trapped in rock during UHP metamorphism. Entrapment in the

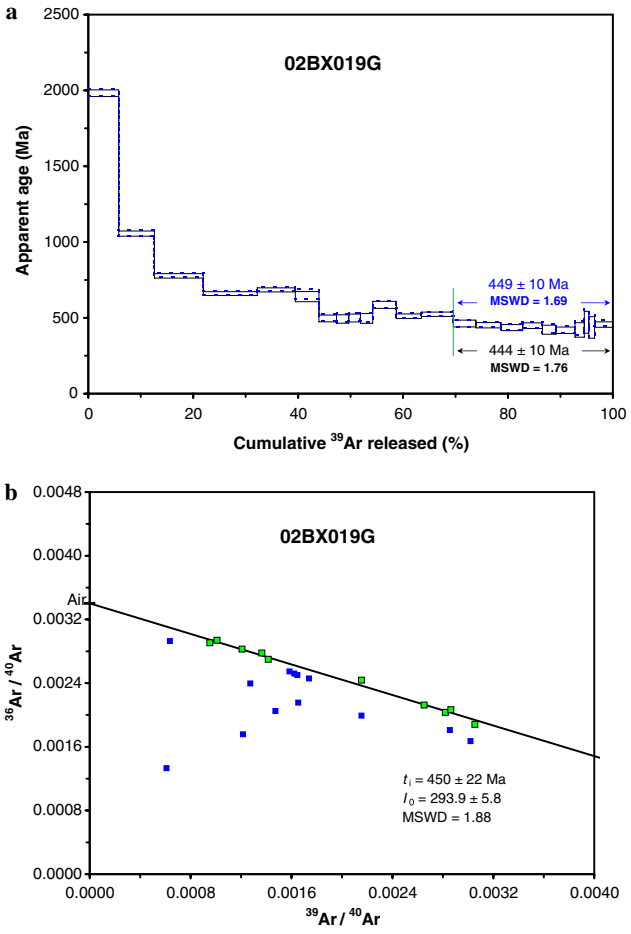


Fig. 6. $^{40}Ar/^{39}Ar$ dating results of garnet 02BX019G by crushing: (a) age spectra; (b) inverse isochron.

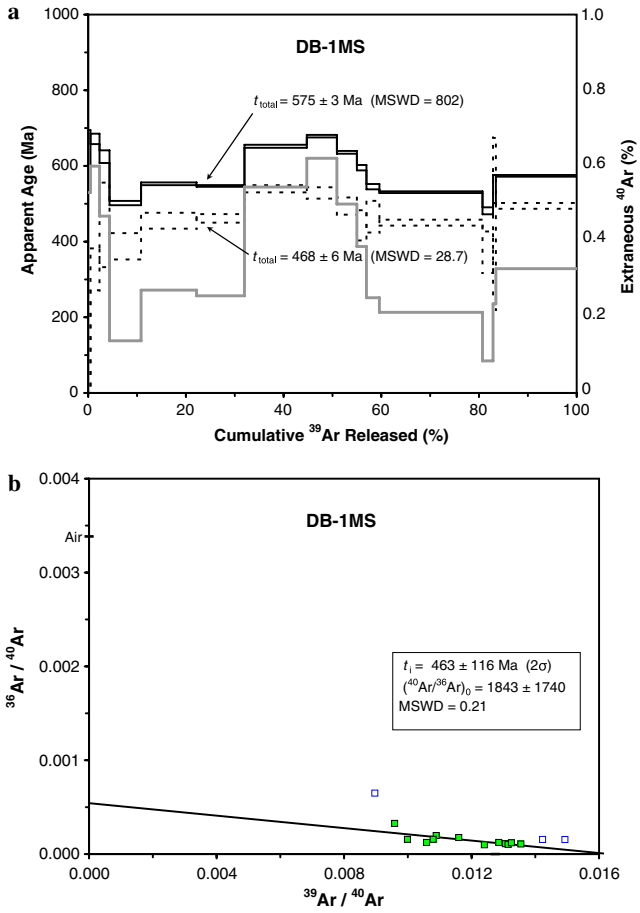


Fig. 7. $^{40}Ar/^{39}Ar$ dating results of phengite DB-1MS by laser stepped heating: (a) age spectra: The real and dotted line age spectra are obtained by correcting non-radiogenic $^{40}Ar$, respectively with the modern atmospheric ratio of 295.5 and with the initial $^{40}Ar/^{36}Ar$ ratio of 1843 ± 1740 of its isochron (b). The grey line shows the ratio of extraneous $^{40}Ar$ ($^{40}Ar_E$) to the in-situ potassium decay radiogenic $^{40}Ar$($^{40}Ar_R$) by ($^{40}Ar^*$–$^{40}Ar_R$)/$^{40}Ar_R$ (here $^{40}Ar^* = {}^{40}Ar_R + {}^{40}Ar_E = {}^{40}Ar_m – 295.5 \times {}^{36}Ar_m$, m: measured data) in each heating step. (b) inverse isochron.

secondary fluid inclusions must have occurred at some time after crystallization of the garnet, and before this fluid phase was lost during progressive decompression. We acknowledge that we cannot distinguish between multiple groups or generations of excess argon-bearing secondary fluid inclusions, i.e., during polyphase metamorphism there may have been several periods favoring a high argon partial pressure in the metamorphic fluid. In the argon data presented here, they are all grouped together as post-dating the early signal that is revealed by prolonged crushing. Only after hundred steps of pestle movements do we observe gas that is apparently a mixture between atmospheric and radiogenic argon, without an apparent contribution of excess $^{40}Ar$. Gas from smaller inclusions is progressively more difficult to release, which is reflected in the observation that it takes progressively more pestle movements (>50 per step) to obtain sufficient gas to perform an analysis. Once we have entered this part of the experiment we observe the gas component corresponding to the age plateaux that we argue to be the contribution of the primary fluid inclusions.

The concordant initial $^{40}Ar/^{36}Ar$ ratios of 292.1–294.5 found for the three garnets, which are within the analytical uncertainty equal to the $^{40}Ar/^{36}Ar$ ratio of the modern atmosphere, support the conclusion from oxygen isotope studies that the protoliths of these eclogites underwent near-surface interaction with meteoric water before the high- to ultrahigh-pressure metamorphism (Yui et al., 1995; Baker et al., 1997; Zheng et al., 1999). If this is the case, then some atmospheric argon may have been incorporated into hydrous minerals during the process of surface water–rock interaction and partly retained in the rock even during the subsequent prograde phase of high-pressure metamorphism, i.e., the period *before* decreased permeability of the rock due to high to ultra-high lithostatic pressures. The results of Fourier transform infrared spectrometer analyses for garnets from Bixiling also demonstrated that all the garnets contain structural water as hydroxyl (OH) with concentration ranging from 164 to 2034 ppm ($H_2O$ wt.) (Sheng et al., 2004).

Within garnet, the most likely present K-rich mineral inclusion is phengite. If perceivable amounts of gases were released from phengite inclusions by crushing, and the phengite trapped inside the garnet is the same as the

Table 4
The key $^{40}Ar/^{39}Ar$ data of the garnets by crushing

| Sample | $J$ | $^{39}Ar$ % in age plateau | Plateau age A[a] (Ma) | Plateau age B[b](Ma) | Isochron age (Ma) | Initial ratio of $^{40}Ar/^{36}Ar$ |
|---|---|---|---|---|---|---|
| DB-1G | 0.004707 | 59.5 | 427 ± 20 | 449 ± 18 | 448 ± 34 | 292.1 ± 4.5 |
| 02BX005G | 0.002015 | 27.2 | 443 ± 31 | 450 ± 31 | 459 ± 58 | 294.5 ± 6.7 |
| 02BX019G | 0.002009 | 30.4 | 444 ± 10 | 449 ± 10 | 450 ± 22 | 293.9 ± 5.8 |

[a] Apply the $^{40}Ar/^{36}Ar$ ratio of the modern atmosphere to exclude the non-radiogenic $^{40}Ar$.
[b] Apply the initial $^{40}Ar/^{36}Ar$ ratio from the isochron lines to exclude the non-radiogenic $^{40}Ar$, respectively.

phengite that was analysed from the bulk rock, than its contribution to the signal would have a profound effect on the shape of the age spectra and on the initial $^{40}Ar/^{36}Ar$ ratio of garnet. In particular, the last steps of the age plateaux and the atmospheric initial $^{40}Ar/^{36}Ar$ ratios would never been obtained. Therefore, we argue that the gas released by crushing must be the contribution mostly from the fluid inclusions and not from mineral inclusions.

Thus, we suggest that the simplest hypothesis is the most likely: the garnet fraction of the Bixiling eclogite was formed during the early Paleozoic, rather than in the Triassic as was implied from previous geochronology. From the garnet compositional data we argue that the garnet formed during UHP metamorphism. The age—although somewhat disturbed—and chemical composition of the eclogite phengite are consistent with this interpretation.

### 5.1.1. Correlations between Cl and K derived Ar isotopes

The correlation between Cl- and K-derived Ar isotopes may help us to identify the different Ar sources in the fluid inclusions (Kelley et al., 1986; Turner and Bannon, 1992; Turner and Wang, 1992; Qiu, 1996; Hu et al., 1998, 2004 Kendrick et al., 2001; Qiu et al., 2002b).

*5.1.1.1. $^{39}Ar_K/^{38}Ar_{Cl}$ vs $^{40}Ar^*/^{38}Ar_{Cl}$.* The plots of $^{39}Ar_K/^{38}Ar_{Cl}$ vs $^{40}Ar^*/^{38}Ar_{Cl}$ based on isotopic analysis of the three garnets by crushing are shown in Fig. 8. The data points of the first several steps show high $^{40}Ar^*/^{38}Ar_{Cl}$ ratios and scatter, and in the case of 02BX005G, no $^{38}Ar_{Cl}$ is released in steps 5–11. As expected, these data points contributing to the age plateaux also define correlation lines with slopes corresponding to ages of 442, 445 and 439 Ma for DB-1G, 02BX005G and 02BX019G, respectively, which are in good agreement with their isochron ages. These correlation lines suggest that the components released by crushing are from the fluid inclusions, in other words, the air-component end member shown in the isochron plots of $^{39}Ar/^{40}Ar$ vs $^{36}Ar/^{40}Ar$ are from the fluid inclusions with garnets, but not an artefact caused by release of argon from the metal of the crusher.

$^{40}Ar/^{39}Ar$ crushing experiments on the hydrothermal quartz (Qiu et al., 2002b) and the UHPM garnet samples show good correlation lines of $^{39}Ar_K/^{38}Ar_{Cl}$ vs $^{40}Ar^*/^{38}Ar_{Cl}$ corresponding to reasonable ages. Therefore, the correlation plot of $^{39}Ar_K/^{38}Ar_{Cl}$ vs $^{40}Ar^*/^{38}Ar_{Cl}$ perhaps provides another approach for obtaining the K-poor sample's ages in crushing experiments.

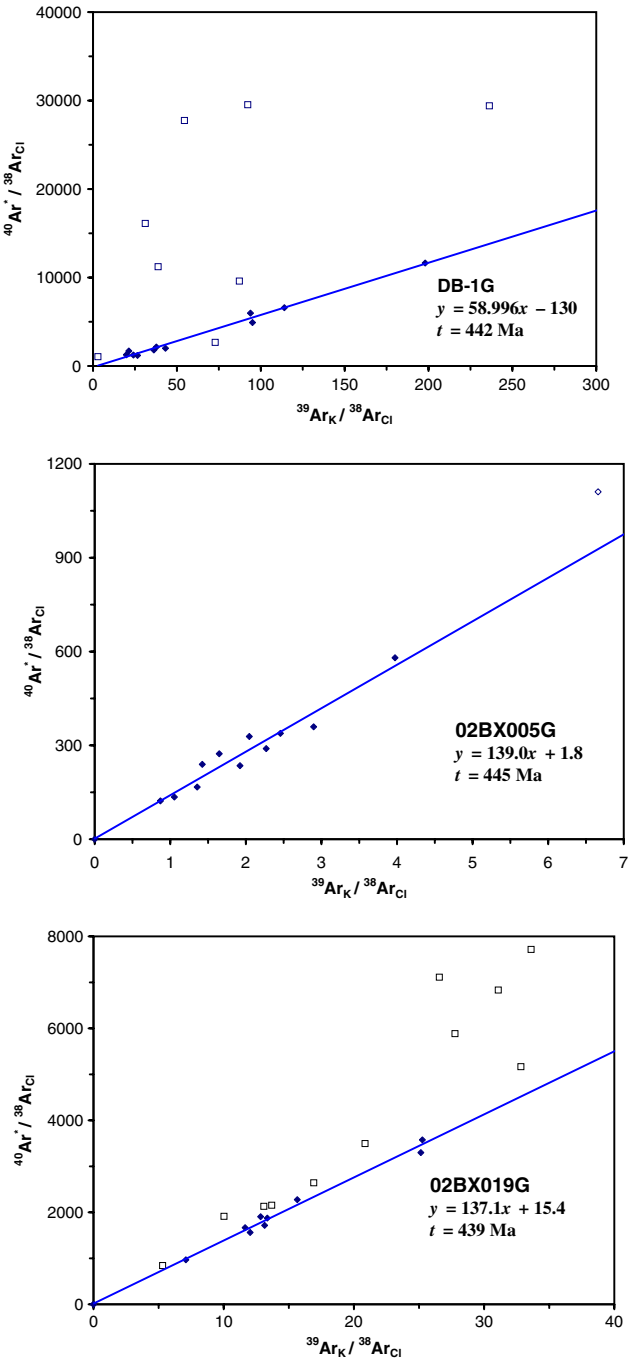


Fig. 8. Plots of $^{39}Ar_K/^{38}Ar_{Cl}$ vs $^{40}Ar^*/^{38}Ar_{Cl}$ based on the $^{40}Ar/^{39}Ar$ data of the garnets by crushing. These data points defining the age plateaux (♦) also define correlation lines with slopes corresponding to ages of 442, 445 and 439 Ma for DB-1G, 02BX005G and 02BX019G, respectively.

*5.1.1.2. $^{38}Ar_{Cl}/^{39}Ar_K$ vs $^{40}Ar^*/^{39}Ar_K$.* The plots of $^{38}Ar_{Cl}/^{39}Ar_K$ vs $^{40}Ar^*/^{39}Ar_K$ based on the $^{40}Ar/^{39}Ar$ data of the garnets by crushing are shown in Fig. 9. The data points of the first several crushing steps show high $^{40}Ar^*/^{39}Ar_K$ ratios and scatter, and in the case of 02BX005G, as noted in the previous paragraph, no $^{38}Ar_{Cl}$ is released in steps 5–11. The $^{40}Ar^*/^{39}Ar_K$ ratios of these steps defining of the age plateaux are relatively constant with respect to the ratios of $^{38}Ar_{Cl}/^{39}Ar_K$. Average values of $^{40}Ar^*/^{39}Ar_K$ yield ages of 443, 455 and 442 Ma for DB-1G, 02BX005G and 02BX019G, respectively, in good agreement with the isochron ages.

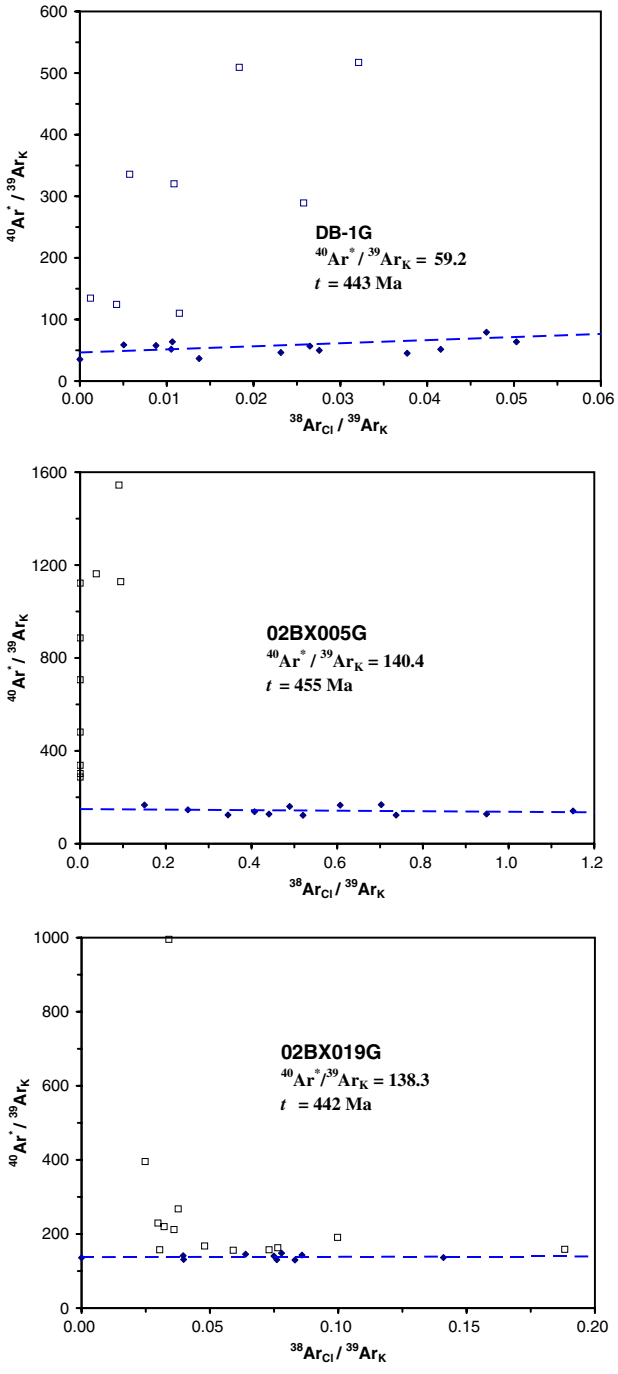


Fig. 9. Plots of $^{38}Ar_{Cl}/^{39}Ar_K$ vs $^{40}Ar^*/^{39}Ar_K$ based on the $^{40}Ar/^{39}Ar$ data of the garnets by crushing. The $^{40}Ar^*/^{39}Ar_K$ ratios of those steps defining the age plateaux (♦) are relatively constant with respect to the ratios of $^{38}Ar_{Cl}/^{39}Ar_K$, corresponding to ages of 443, 455 and 442 Ma for DB-1G, 02BX005G and 02BX019G, respectively.

In cases where the $^{40}Ar^*/^{39}Ar_K$ ratios clearly correlate with $^{38}Ar_{Cl}/^{39}Ar_K$ratios, the intercepts of $^{40}Ar^*/^{39}Ar_K$ will correspond to reasonable ages (Qiu et al., 2002b).

*5.1.2. Application of the $^{40}Ar/^{39}Ar$ crushing technique*

Most of the crushed powder particles resulting from crushing experiments after 3300 pestle drops range in size from 0.5 to 0.05 μm when measured by SEM. This size range would suggest that most of the fluid inclusions within garnet observed by optical microscope should have been extracted by our crushing apparatus. In our experience, samples where fluid inclusions were easily found by microscope usually yielded reasonable $^{40}Ar/^{39}Ar$ isochron ages by crushing. Because potassium is generally present in the fluid inclusions with a range in $K/^{40}Ar$ ratios, the data points cover a wide range on the isochron plots of $^{36}Ar/^{40}Ar$ vs $^{39}Ar/^{40}Ar$. The initial $^{40}Ar/^{36}Ar$ ratios may indicate whether excess $^{40}Ar$ exists within the fluid inclusions or not. Therefore, the $^{40}Ar/^{39}Ar$ crushing technique could be applied to date hydrothermal and metamorphic K-poor minerals containing fluid inclusions or to investigate the fluid evolution during mineralization or metamorphism. As both $^{40}K$ and $^{40}Ar$ are encapsulated in the inclusion, retention of argon is a function of the diffusivity of argon in garnet, which we assume is very low. Potassium may well be in solution in these aqueous fluids, the argon is simply trapped in the inclusion either in a gas bubble or dissolved in the liquid.

*5.2. Phengite age spectrum*

The initial $^{40}Ar/^{36}Ar$ ratio of $1840 \pm 1740$ of phengite DB-1MS is obviously much higher than that of the modern atmosphere, showing the presence of extraneous $^{40}Ar$ within the phengite. We take the isochron age of 448 Ma of the coexisting garnet by crushing (Fig. 4b) as its real age to calculate ratios of extraneous $^{40}Ar$ ($^{40}Ar_E$) to the in situ potassium decay radiogenic $^{40}Ar$ ($^{40}Ar_R$) by $(^{40}Ar^*-^{40}Ar_R)/^{40}Ar_R$ with $^{40}Ar^* = {}^{40}Ar_R + {}^{40}Ar_E = {}^{40}Ar_m - 295.5 \times {}^{36}Ar_m$, m: measured data.

In total the $^{40}Ar_E/^{40}Ar_R$ ratio is about 1/3 within the phengite, and the $^{40}Ar_E/^{40}Ar_R$ ratios are quite inhomogeneous from 0.08 to 0.62 (Fig. 7a, the grey line) in the heating steps.

Two possible sources of extraneous $^{40}Ar$ exist: (1) inherited $^{40}Ar$ from protolith (Giorgis et al., 2000); (2) excess $^{40}Ar$ in the fluid during retrograde metamorphism incorporating into the phengite crystal lattice by diffusion. The inhomogeneous distribution of extraneous $^{40}Ar$ within the phengite causes the abnormal high $^{40}Ar/^{39}Ar$ apparent ages and the data point scatter on the isochron diagrams.

In terms of the occurrence of extraneous $^{40}Ar$ within garnet and phengite, we infer that excess $^{40}Ar$ together with fluid entered the minerals during the retrograde

metamorphism. High partial pressures of argon in the metamorphic fluid during (U)HP metamorphism may have caused $^{40}Ar$ to diffuse into interlayer sites in the phengite crystal structure. In contrast, the compact crystal structure of garnet and its resultant low argon diffusivity prevented the intake of excess $^{40}Ar$ into the garnet crystal lattice, with the exception for argon trapped along micro-cracks where secondary fluid inclusions are distributed. Thus, the lack of excess $^{40}Ar$ that is found within garnet by $^{40}Ar/^{39}Ar$ UV-laser ablation analysis (Giorgis et al., 2000) is perhaps a function of the very low diffusivity of argon in garnet and the high content of excess argon in phengite is a function of the higher diffusivity of argon in phengite.

### 5.3. The age of metamorphism of the Bixiling eclogite

In a recent study using a SHRIMP II instrument, a series of zircon samples from the Bixiling eclogite and granitic gneiss were dated using the U/Pb technique. The weighted mean ages of the SHRIMP zircon U–Pb ages of zircons from the dark coloured eclogite, light coloured eclogite and granitic gneiss are $455 \pm 4$, $452 \pm 3$ and $442 \pm 2$ Ma, respectively (cited in Yang et al., 2002). These ages are in good agreement with each other, and in excellent agreement with the $^{40}Ar/^{39}Ar$ isochron age of the primary fluid inclusions of the garnets by crushing found in the present study. Whereas the U/Pb age of low-U zircons can be determined with high analytical precision, the link between zircon growth and the PT*t* history of the rock is not always straightforward. Zircon may grow during primary magmatic crystallization, and during subsequent metamorphic events. As a consequence, pre-Triassic zircon ages until now could be dismissed as recording various stages of protolith history. In contrast, with the $^{40}Ar/^{39}Ar$ technique, age information is obtained on minerals that define the metamorphic assemblage. The phengite ages by themselves are not strong evidence for an older metamorphic age of Bixiling because of the potential presence of inherited or excess $^{40}Ar$. Our garnet results, however, demonstrate that within the garnets a reservoir is preserved that also records the earlier Paleozoic age, and at the same time due to its isochron relation can only be interpreted as a mixing line between radiogenic argon and atmospheric argon. Thus, from our work we contend that the eclogite mineral assemblage phengite–garnet formed during the early Paleozoic and not in the Triassic. This information in combination with the zircon U–Pb (Yang et al., 2002) and other previous data in Table 1, represents strong evidence that Bixiling has had a complex thermal history recording both Paleozoic and Triassic metamorphic ages.

In summary, we suggest that while the effects of Triassic metamorphism in the Dabie–Sulu terrain are undeniably profound, the largest of the Dabie eclogite bodies, Bixiling, shows evidence that it was formed earlier, with primary igneous ages perhaps as old as the late Precambrian, and that the (U-)HP mineralogy first formed in the early Paleozoic, i.e., well before the dominant Triassic (U-)HP event.

On the basis of SHRIMP U–Pb zircon data combined with mineral and whole-rock Sm–Nd, $^{40}Ar/^{39}Ar$ and $^{207}Pb/^{206}Pb$ data, Jian et al. (2000) concluded that Xiongdian eclogite in northwestern Dabieshan formed between 424 and 480 Ma. Gao et al. (2002) also obtained SHRIMP U–Pb zircon ages of $461 \pm 7$ Ma for the Yingshan eclogite and $449 \pm 14$ Ma for the Xiongdian eclogite. Coesite-bearing zircons from a Qinglongshan eclogite in the south Sulu belt yielded early Paleozoic UHPM ages of $441 \pm 9$, $449 \pm 9$ and $442 \pm 9$ Ma, whereas the core of a zircon containing plagioclase and apatite inclusions gave a protolith age of $761 \pm 13$ Ma (Yang et al., 2005). Paleozoic SHRIMP U–Pb zircon ages of 505–455 Ma were also reported for the coesite-bearing paragneisses in drill holes at Donghai, southwestern Sulu terrane (Liu et al., 2005). In the last decade, ultra-high-pressure and high-pressure metamorphism in eclogites, gneisses and granulites was also found along the belt from Dabieshan, Qinling to northern Qaidam and Altyn Tagh (the Central Orogenic Belt of China) (Fig. 10). These rocks were all formed during a metamorphic event around 450–500 Ma. For the Altyn Tagh eclogites, the Sm–Nd isotopic data yield a whole rock-garnet-omphacite isochron age of $500 \pm 10$ Ma, and U–Pb zircon ages from the same eclogite show four populations that are near concordant, giving a weighted mean age of $504 \pm 5$ Ma (Zhang et al., 2001). For the Altyn Tagh granitoid gneiss, the SHRIMP zircon ages of 484–491 Ma were obtained (Zhang et al., 2004). For the eclogites at the northern margin of Qaidam basin, the weighted mean zircon U–Pb age of $495 \pm 7$ Ma, SHRIMP U–Pb ages of 486–488 Ma, and $^{40}Ar/^{39}Ar$ isochron age for phengite of 466–477 Ma were obtained (Zhang et al., 2000, 2005). Coesite-bearing zircons from a North Qaidam gneiss yielded UHP metamorphic ages of $452 \pm 13.8$ Ma (Yang et al., 2005). For the northern Qinling granulite, LA-ICP-MS zircon U–Pb age of $485 \pm 3$ Ma was reported (Chen et al., 2004). Hacker et al. (1998) questioned the prevailing assumption that the Triassic ages of zircons from Qinling-Dabie formed at ultrahigh pressure and proposed instead that they reflect late retrogression at crustal pressures following the bulk of exhumation. Hacker et al. (1998) also agreed with the interpretation of ~480 to 400 Ma as the metamorphic ages occurred in Qinling.

Thus, our new results support an emerging picture that early Paleozoic (U-)HP metamorphism was widespread in the Central Orogenic Belt of China.

## 6. Conclusions

The main new findings from this study are summarized as follows:

(1) The $^{40}Ar/^{39}Ar$ crushing technique has been applied to garnets from the Bixiling UHPM eclogites. The method appears to successfully deconvolve argon from different sources within the garnets. Argon released early in the crushing experiments yields anomalously old

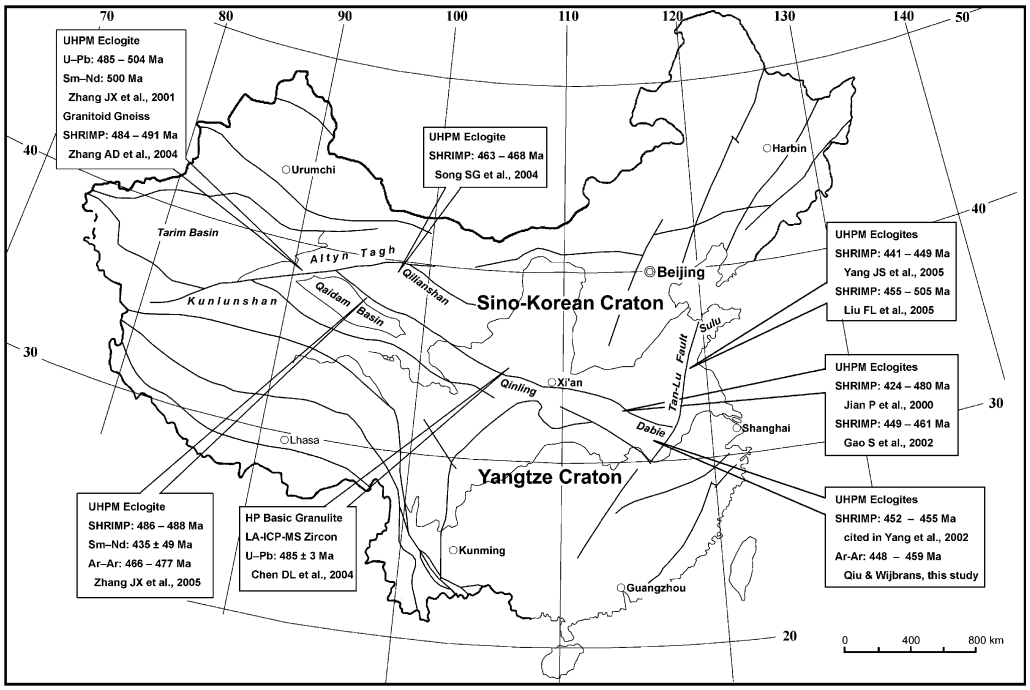


Fig. 10. Simplified geological map showing the Caledonian ages recently obtained from the eclogites, gneiss and granulite in the Central Orogenic Belt of China.

ages indicative of excess argon, whereas argon released in later parts of the experiments yields relatively concordant ages that do not appear to be affected by excess argon.

(2) Excess argon released early in the experiments are is interpreted to be sourced from relatively large secondary fluid-inclusions, which were formed subsequent to initial UHP metamorphism and garnet crystallisation. Radiogenic argon released in later parts of the experiments in interpreted to derive from small primary fluid-inclusions trapped during garnet growth. The $^{40}Ar/^{39}Ar$ ages derived from these primary fluid-inclusions are therefore regarded as approximating the time of garnet growth during UHP metamorphism. The absence of excess argon in the primary fluid inclusions indicates that excess argon was not present during original crystallisation of the garnets at eclogite-facies conditions, but entered the garnets during later fluid activity subsequent to garnet crystallisation.

(3) The concordant $^{40}Ar/^{39}Ar$ plateau ages and isochron ages of ca. 450 Ma of the garnets DB-1G, 02BX005G and 02BX019G by crushing are in excellent agreement with the SHRIMP zircon U–Pb ages of the Bixiling eclogites and granitic gneiss. The geological significance of these early Paleozoic ages should be further investigated. However, as these ages were obtained from eclogite-grade metamorphic garnets, we contend that we are in fact dealing with a metamorphic signal rather than with a signal related to the protolith of these eclogites.

## Acknowledgments

We thank Dr. T. Chacko, Dr. Geoff Fraser, Dr. Jim K. W. Lee and an anonymous reviewer for their comments that substantially improved this manuscript. Dr. Randell Stephenson kindly read the manuscript and suggested improvements to the language. We are greatly indebted to Profs. Y.F. Zheng, S.G. Li and C.T. Zhou and Dr. Y.B. Wu for their introductions to the Dabieshan field area. It is a pleasure for us to thank Prof. P.A.M. Andriessen and Prof. J.L.R. Touret for their supports of this study. Mr. O. Postma, Mr. R. van Elsas, Prof. G. Davies and Dr. F.J.C. Peeters kindly offered us help in mineral separation, making of crushing apparatus and the $^{40}Ar/^{39}Ar$ experiments. Mrs. W. Koot and Mr. W.J. Lustenhouwer kindly helped us with thin-section polishing and EPMA analyses. The research was funded by the project of the National Natural Science Foundation of China (40272039), the collaboration project between the Chinese Academy of Sciences (KZCX2-SW117 & GIGCX-03-01) and the Royal Netherlands Academy of Arts and Sciences (01CDP026).

*Associate editor:* Thomas Chacko

## References

Ames, L., Zhou, G.Z., Xiong, B.C., 1996. Geochronology and isotopic character of ultrahigh-pressure metamorphism with implications for collision of the Sino-Korean and Yangtze cratons, central China. *Tectonics* **15** (2), 472–489.

Arnaud, N.O., Kelley, S.P., 1995. Evidence for excess argon during high-pressure metamorphism in the Dora-Maira Massif (Western Alps,

Italy), using an ultra-violet laser-ablation microprobe $^{40}Ar$–$^{39}Ar$ Technique. *Contrib. Mineral. Petrol.* **121** (1), 1–11.

Baker, J., Matthews, A., Mattey, D., Rowley, D., Xue, F., 1997. Fluid-rock interactions during ultra-high pressure metamorphism, Dabie Shan, China. *Geochim. Cosmochim. Acta* **61** (8), 1685–1696.

Boundy, T.M., Hall, C.M., Li, G., Essene, E.J., Halliday, A.N., 1997. Fine-scale isotopic heterogeneities and fluids in the deep crust: a $^{40}Ar/^{39}Ar$ laser ablation and TEM study of muscovites from a granulite-eclogite transition zone. *Earth Planet. Sci. Lett.* **148** (1–2), 223–242.

Cao, R., Zhu, S., 1995. A U–Pb and $^{40}Ar/^{39}Ar$ geochronologic study of Bixiling coesite-bearing eclogite from Anhui Province, China. *Geochimica* **24** (2), 152–161.

Cao, R., Zhu, S., 1996. The Dabieshan coesite-bearing eclogite terrain; a late Archaean ultra-high-pressure metamorphic belt. *Acta Geol. Sin.-Engl. Ed.* **9** (1), 46–58.

Carrapa, B., Wijbrans, J., Bertotti, G., 2003. Episodic exhumation in the Western Alps. *Geology* **31** (7), 601–604.

Chavagnac, V., Jahn, B., 1996. Coesite-bearing eclogites from the Bixiling Complex, Dabie Mountains, China: Sm–Nd ages, geochemical characteristics and tectonic implications. *Chem. Geol.* **133** (1–4), 29–51.

Chen, D.L., Liu, L., Sun, Y., Zhang, A.D., Liu, X.M., Luo, J.H., 2004. LA-ICP-MS zircon U–Pb dating for high-pressure basic granulite from North Qinling and its geological significance. *Chin. Sci. Bull.* **49** (21), 2296–2304.

Cheng, Y.Q., Liu, D.Y., Williams, I.S., Jian, P., Zhuang, Y.X., Gao, T.S., 2000. SHRIMP U–Pb dating of zircons of a dark eclogite and a garnet-bearing gneissic granitic rock from Bixiling, Eastern Dabie area, Anhui Province: isotope chronological evidence of neoproterozoic UHP metamorphism. *Acta Geol. Sin.-Engl. Ed.* **74** (4), 748–765.

Cong, B.L., Wang, Q.C., 1999. The Dabie-Sulu UHP rocks belt: review and prospect. *Chin. Sci. Bull.* **44** (12), 1074–1086.

Dunai, T.J., Roselieb, K., 1996. Sorption and diffusion of helium in garnet: implications for volatile tracing and dating. *Earth Planet. Sci. Lett.* **139** (3–4), 411–421.

Dunlap, W.J., Kronenberg, A.K., 2001. Argon loss during deformation of micas: constraints from laboratory deformation experiments. *Contrib. Mineral. Petrol.* **141** (2), 174–185.

Ellis, D.J., Green, D.H., 1979. An experimental study of the effect of Ca upon garnet-clinopyroxene Fe–Mg exchange equilibria. *Contrib. Mineral. Petrol.* **71** (1), 13–22.

Fu, B., Touret, J.L.R., Zheng, Y.F., 2001. Fluid inclusions in coesite-bearing eclogites and jadeite quartzite at Shuanghe, Dabie Shan (China). *J. Metamorph. Geol.* **19** (5), 529–545.

Fu, B., Zheng, Y.F., Touret, J.L.R., 2002. Petrological, isotopic and fluid inclusion studies of eclogites from Sujiahe, NW Dabie Shan (China). *Chem. Geol.* **187** (1–2), 107–128.

Fu, B., Touret, J.L.R., Zheng, Y.F., Jahn, B.M., 2003. Fluid inclusions in granulites, granulitized eclogites and garnet clinopyroxenites from the Dabie-Sulu terranes, Eastern China. *Lithos* **70** (3–4), 293–319.

Gao, S., Qiu, Y.M., Ling, W.L., McNaughton, N.J., Zhang, B.R., Zhang, G.W., Zhang, Z.M., Zhong, Z.Q., Suo, S.T., 2002. SHRIMP single zircon U–Pb geochronology of eclogites from Yingshan and Xiongdian. *Earth Sci.-J. China Univ. Geosci.* **27** (5), 558–564.

Giorgis, D., Cosca, M., Li, S.G., 2000. Distribution and significance of extraneous argon in UHP eclogite (Sulu terrain, China): insight from in situ $^{40}Ar/^{39}Ar$ UV-laser ablation analysis. *Earth Planet. Sci. Lett.* **181** (4), 605–615.

Hacker, B.R., Ratschbacher, L., Webb, L., Ireland, T., Walker, D., Shuwen, D., 1998. U/Pb zircon ages constrain the architecture of the ultrahigh-pressure Qinling-Dabie Orogen, China. *Earth Planet. Sci. Lett.* **161** (1–4), 215–230.

Hacker, B.R., Wang, Q.C., 1995. Ar/Ar geochronology of ultrahigh-pressure metamorphism in Central China. *Tectonics* **14** (4), 994–1006.

Hannula, K.A., McWilliams, M.O., 1995. Reconsideration of the age of blueschist facies metamorphism on the Seward Peninsula, Alaska, based on phengite $^{40}Ar/^{39}Ar$ results. *J. Metamorph. Geol.* **13** (1), 125–139.

Hu, R.Z., Burnard, P.G., Turner, G., Bi, X.W., 1998. Helium and Argon isotope systematics in fluid inclusions of Machangqing copper deposit in west Yunnan province, China. *Chem. Geol.* **146** (1–2), 55–63.

Hu, R.Z., Burnard, P.G., Bi, X.W., Zhou, M.F., Pen, J.T., Su, W.C., Wu, K.X., 2004. Helium and argon isotope geochemistry of alkaline intrusion-associated gold and copper deposits along the Red River-Jinshajiang fault belt, SW China. *Chem. Geol.* **203** (3–4), 305–317.

Hu, S.-L., Hao, J., Li, Y.-J., Dai, T.-M., Pu, Z.-P., 1999. Laser porobe $^{40}Ar$–$^{39}Ar$ isochron age of eclogite from Bixiling, Dabie UHP orogenic belt. *Scientia Geologica Sinica* **34** (4), 427–431.

Jian, P., Liu, D.Y., Yang, W.R., Williams, I.S., 2000. Petrographic and SHRIMP studies of zircons from the Caledonian Xiongdian Eclogite, Northwestern Dabie Mountains. *Acta Geol. Sin.-Engl. Ed.* **74** (4), 766–773.

Jian, P., Ye, B.D., Li, Z.C., 1994. The eclogite isotopic geochronology and PTt path of Dabieshan. In: Chen, H.S. (Ed.), *Studies of Isotope Geochemistry*. Zhejiang Univ. Press, pp. 177–195.

Kelley, S., 2002. Excess argon in K–Ar and Ar–Ar geochronology. *Chem. Geol.* **188** (1–2), 1–22.

Kelley, S., Turner, G., Butterfield, A.W., Shepherd, T.J., 1986. The source and significance of argon isotopes in fluid inclusions from areas of mineralization. *Earth Planet. Sci. Lett.* **79** (3–4), 303–318.

Kendrick, M.A., Burgess, R., Pattrick, R.A.D., Turner, P.G., 2001. Halogen and Ar–Ar age determinations of inclusions within quartz veins from porphyry copper deposits using complementary noble gas extraction techniques. *Chem. Geol.* **177** (3–4), 351–370.

Koppers, A.A.P., 2002. ArArCALC—software for $^{40}Ar/^{39}Ar$ age calculations. *Comput. Geosci.* **28** (5), 605–619.

Krogh, E.J., 1988. The garnet-clinopyroxene Fe–Mg geothermometer—a reinterpretation of existing experimental-data. *Contrib. Mineral. Petrol.* **99** (1), 44–48.

Li, S.G., Jagoutz, E., Chen, Y.Z., Li, Q.L., 2000. Sm–Nd and Rb–Sr isotopic chronology and cooling history of ultrahigh pressure metamorphic rocks and their country rocks at Shuanghe in the Dabie Mountains, Central China. *Geochim. Cosmochim. Acta* **64** (6), 1077–1093.

Li, S.G., Wang, S.S., Chen, Y.H., Liu, D.L., Qiu, J., Zhou, H.X., Zhang, Z.M., 1994. Excess argon in phengite from eclogite—evidence from dating of eclogite minerals by Sm–Nd, Rb–Sr and $^{40}Ar/^{39}Ar$ Methods. *Chem. Geol.* **112** (3–4), 343–350.

Li, S.G., Xiao, Y.L., Liou, D.L., Chen, Y.Z., Ge, N.J., Zhang, Z.Q., Sun, S.S., Cong, B.L., Zhang, R.Y., Hart, S.R., Wang, S.S., 1993. Collision of the North China and Yangtse blocks and formation of coesite-bearing eclogites —timing and processes. *Chem. Geol.* **109** (1–4), 89–111.

Lippolt, H.J., Hess, J., 1994. Compilation of K–Ar measurements on HD–B1 standard biotite 1994 status report. In: Odin, G.S. (Ed.), *Phanerozoic Timescale*, vol. 12. IUGS Subcomission on Geochronology, pp. 18–23.

Liu, F.L., Liou, J.G., Xu, Z.Q., 2005. U–Pb SHRIMP ages recorded in the coesite-bearing zircon domains of paragneisses in the Southwestern Sulu terrane, Eastern China: new interpretation. *Am. Miner.* **90** (5–6), 790–800.

Liu, R.X., Fan, Q.C., Li, H.M., Zhang, Q., Zhao, D.S., Ma, B.L., 1995. The nature of protolith of Bixiling garnet peridotite-eclogite massif in Dabie Mountains and the implication of its isotopic geochronology. *Acta Petrologica Sinica* **11** (3), 243–255.

McDougall, I., Harrison, T.M., 1999. *Geochronology and thermochronology by the $^{40}Ar/^{39}Ar$ method*. Oxford University Press.

Okay, A.I., 1993. Petrology of a diamond and coesite-bearing metamorphic terrain—Dabie Shan, China. *Eur. J. Mineral.* **5** (4), 659–675.

Okay, A.I., Sengor, A.M.C., Satir, M., 1993. Tectonics of an ultrahigh-pressure metamorphic terrane—the Dabie-Shan Tongbai-Shan Orogen, China. *Tectonics* **12** (6), 1320–1334.

Powell, R., 1985. Regression diagnostics and robust regression in geothermometer geobarometer calibration— the garnet clinopyroxene geothermometer revisited. *J. Metamorph. Geol.* **3** (3), 231–243.

Qiu, H.N., 1996. $^{40}Ar$–$^{39}Ar$ dating of the quartz samples from two mineral deposits in Western Yunnan (SW China) by crushing in vacuum. *Chem. Geol.* **127** (1–3), 211–222.

Qiu, H.N., Wijbrans, J.R., Li, X.H., Zhu, B.Q., Zhu, C.L., Zeng, B.C., 2002a. New $^{40}Ar$–$^{39}Ar$ evidence for ore-forming process during Jinning-Chengjiang period in Dongchuan type copper deposits, Yunnan. (in Chinese with English abstract). *Mineral Deposits* **21** (2), 129–136.

Qiu, H.N., Zhu, B.Q., Sun, D.Z., 2002b. Age significance interpreted from $^{40}Ar$–$^{39}Ar$ dating of quartz samples from the Dongchuan copper deposits, Yunnan, SW China, by crushing and heating. *Geochem. J.* **36** (5), 475–491.

Rowley, D.B., Xue, F., Tucker, R.D., Peng, Z.X., Baker, J., Davis, A., 1997. Ages of ultrahigh pressure metamorphism and protolith orthogneisses from the eastern Dabie Shan: U/Pb zircon geochronology. *Earth Planet. Sci. Lett.* **151** (3–4), 191–203.

Ruffet, G., Feraud, G., Balevre, M., Kienast, J.R., 1995. Plateau ages and excess argon in phengites—an $^{40}Ar$–$^{39}Ar$ laser probe study of alpine micas (Sesia Zone, Western Alps, Northern Italy). *Chem. Geol.* **121** (1–4), 327–343.

Ruffet, G., Gruau, G., Ballevre, M., Feraud, G., Philippot, P., 1997. Rb–Sr and $^{40}Ar$–$^{39}Ar$ laser probe dating of high-pressure phengites from the Sesia zone (Western Alps): underscoring of excess argon and new age constraints on the high-pressure metamorphism. *Chem. Geol.* **141** (1–2), 1–18.

Scaillet, S., 1996. Excess $^{40}Ar$ transport scale and mechanism in high-pressure phengites: a case study from an eclogitized metabasite of the Dora-Maira nappe, western Alps. *Geochim. Cosmochim. Acta* **60** (6), 1075–1090.

Scaillet, S., 1998. K–Ar ($^{40}Ar/^{39}Ar$) Geochronology of ultrahigh pressure rocks. In: Hacker, B.R., Liou, G. (Eds.), *When continents collide: geodynamics and geochemistry of ultrahigh-pressure rocks*. Kluwer Academic Publishers.

Scaillet, S., Feraud, G., Ballevre, M., Amouric, M., 1992. Mg/Fe and (Mg,Fe)Si–$Al_2$ compositional control on argon behavior in high-pressure white micas—a $^{40}Ar/^{39}Ar$ continuous laser-probe study from the Dora-Maira Nappe of the Internal Western Alps, Italy. *Geochim. Cosmochim. Acta* **56** (7), 2851–2872.

Sheng, Y.M., Xia, Q.K., Yang, X.Z., 2004. Heterogeneity of water in UHP eclogites from Bixiling in Dabieshan: evidence from garnet. *Chin. Sci. Bull.* **49** (5), 481–486.

Sherlock, S., Kelley, S., 2002. Excess argon evolution in HP–LT rocks: a UVLAMP study of phengite and K-free minerals, NW Turkey. *Chem. Geol.* **182** (2–4), 619–636.

Sherlock, S.C., Arnaud, N.O., 1999. Flat plateau and impossible isochrons: apparent $^{40}Ar$–$^{39}Ar$ geochronology in a high-pressure terrain. *Geochim. Cosmochim. Acta* **63** (18), 2835–2838.

Su, W., You, Z.D., Cong, D.L., Ye, K., Zhong, Z.Q., 2002. Cluster of water molecules in garnet from ultrahigh-pressure eclogite. *Geology* **30** (7), 611–614.

Tonarini, S., Villa, I.M., Oberli, F., Meier, M., Spencer, D.A., Pognante, U., Ramsay, J.G., 1993. Eocene age of eclogite metamorphism in Pakistan Himalaya—implications for India Eurasia Collision. *Terr. Nova* **5** (1), 13–20.

Turner, G., Bannon, M.P., 1992. Argon isotope geochemistry of inclusion fluids from granite-associated mineral veins in Southwest and Northeast England. *Geochim. Cosmochim. Acta* **56** (1), 227–243.

Turner, G., Wang, S.S., 1992. Excess argon, crustal fluids and apparent isochrons from crushing K-Feldspar. *Earth Planet. Sci. Lett.* **110** (1–4), 193–211.

Wan, Y.S., Li, R.W., Wilde, S.A., Liu, D.Y., Chen, Z.Y., Yan, L., Song, T.R., Yin, X.Y., 2005. UHP metamorphism and exhumation of the Dabie Orogen, China: evidence from SHRIMP dating of zircon and monazite from a UHP granitic gneiss cobble from the Hefei Basin. *Geochim. Cosmochim. Acta* **69** (17), 4333–4348.

Wang, S.S., Ge, N.J., Sang, H.Q., Qiu, J., 2000. Genesis of excess argon in phengite and significance of $^{40}Ar$–$^{39}Ar$ age spectra for omphacite: a case study on UHP eclogite of South Dabie terrain, China. *Chin. Sci. Bull.* **45** (15), 1345–1351.

Wijbrans, J.R., Pringle, M.S., Koppers, A.A.P., Scheveers, R., 1995. Argon geochronology of small samples using the Vulkaan Argon laserprobe. *Proc. K. Ned. Akad. Wet.-Biol. Chem. Geol. Phys. Med. Sci.* **98** (2), 185–218.

Xiao, Y.L., Hoefs, J., van den Kerkhof, A.M., Fiebig, J., Zheng, Y.F., 2000. Fluid history of UHP metamorphism in Dabie Shan, China: a fluid inclusion and oxygen isotope study on the coesite-bearing eclogite from Bixiling. *Contrib. Mineral. Petrol.* **139** (1), 1–16.

Xie, Z., Chen, J.F., 2005. Multi-stage evolution of the orthogneiss from Baizhangyan, North Dabie, China. Goldschmidt Conference Abstracts 2005 Geochim. Cosmochim. Acta 69(10, Suppl. 1), A295.

Xu, S.T., Liu, Y.C., Chen, G.B., Compagnoni, R., Rolfo, F., He, M.C., Liu, H.F., 2003. New finding of micro-diamonds in eclogites from Dabie-Sulu region in Central-Eastern China. *Chin. Sci. Bull.* **48** (10), 988–994.

Xu, S.T., Okay, A.I., Ji, S.Y., Sengor, A.M.C., Wen, S., Liu, Y.C., Jiang, L.L., 1992. Diamond from the Dabie-Shan metamorphic rocks and its implication for tectonic setting. *Science* **256** (5053), 80–82.

Yang, J.S., Liu, F.L., Wu, C.L., Xu, Z.Q., Shi, R.D., Chen, S.Y., Deloule, E., Wooden, J.L., 2005. Two ultrahigh-pressure metamorphic events recognized in the Central Orogenic Belt of China: evidence from the U–Pb dating of coesite-bearing zircons. *Int. Geol. Rev.* **47** (4), 327–343.

Yang, W.R., Jian, P., 1998. Geochronological study of caledonian granulite and high-pressure gneiss in the Dabie Mountains. *Acta Geol. Sin.-Engl. Ed.* **72** (3), 264–270.

Yang, W.R., Jian, P., Han, Y.J., 2002. Determination and significance of Caledonian high-pressure and ultrahigh-pressure metamorphism in Dabie Orogen. *Earth Science Frontiers (China University of Geosciences, Beijing)* **9** (4), 273–283.

Yang, W.R., You, Z.D., Han, Y.J., 1995. The tectonic characteristics and evolution of the Qinling-Dabie high-pressure and ultrahigh-pressure metamorphic belt, Central China. (in Chinese). *Geological Journal of Universities* **1** (2), 53–64.

Ye, K., Cong, B.L., Ye, D.I., 2000. The possible subduction of continental material to depths greater than 200 km. *Nature* **407** (6805), 734–736.

Ye, K., Liou, J.B., Cong, B.L., Maruyama, S., 2001. Overpressures induced by coesite-quartz transition in zircon. *Am. Miner.* **86** (10), 1151–1155.

Ye, K., Liu, J.B., Cong, B.L., Ye, D.N., Xu, P., Omori, S., Maruyama, S., 2002. Ultrahigh-pressure (UHP) low-Al titanites from carbonate-bearing rocks in Dabieshan-Sulu UHP terrane, Eastern China. *Am. Miner.* **87** (7), 875–881.

Yui, T.F., Rumble, D., Lo, C.H., 1995. Unusually low delta-o-18 ultrahigh-pressure metamorphic rocks from the Sulu terrain, Eastern China. *Geochim. Cosmochim. Acta* **59** (13), 2859–2864.

Zhang, A.D., Liu, L., Sun, Y., Chen, D.L., Wang, Y., Luo, J.H., 2004. SHRIMP U–Pb zircon ages for the UHP metamorphosed granitoid gneiss in Altyn Tagh and their geological significance. *Chin. Sci. Bull.* **49** (23), 2527–2532.

Zhang, J.X., Yang, J.S., Mattinson, C.G., Xu, Z.Q., Meng, F.C., Shi, R.D., 2005. Two contrasting eclogite cooling histories, North Qaidam HP/UHP terrane, Western China: petrological and isotopic constraints. *Lithos* **84** (1–2), 51–76.

Zhang, J.X., Yang, J.S., Xu, Z.Q., Zhang, Z.M., Chen, W., Li, H.B., 2000. Peak and retrograde age of eclogites at the northern margin of Qaidam basin northwestern China: evidences from U–Pb and Ar–Ar dates. *Geochimica* **29** (5), 217–222.

Zhang, J.X., Zhang, Z.M., Xu, Z.Q., Yang, J.S., Cui, J.W., 2001. Petrology and geochronology of eclogites from the western segment of the Altyn Tagh, Northwestern China. *Lithos* **56** (2–3), 187–206.

Zhang, R.Y., Liou, J.G., Cong, B.L., 1995. Talc-, magnesite- and Ti-clinohumite-bearing ultrahigh-pressure meta-mafic and ultramafic complex in the Dabie Mountains, China. *J. Petrol.* **36** (4), 1011–1037.

Zheng, Y.F., 1993a. Calculation of oxygen-isotope fractionation in hydroxyl-bearing silicates. *Earth Planet. Sci. Lett.* **120** (3–4), 247–263.

Zheng, Y.F., 1993b. Calculation of oxygen isotope fractionation in anhydrous silicate minerals. *Geochim. Cosmochim. Acta* **57** (5), 1079–1091.

Zheng, Y.F., Fu, B., Xiao, Y.L., Li, Y.L., Gong, B., 1999. Hydrogen and oxygen isotope evidence for fluid-rock interactions in the stages of pre- and post-UHP metamorphism in the Dabie Mountains. *Lithos* **46** (4), 677–693.